Electrical Power and Energy Systems 174 (2026) 111524

Contents lists available at ScienceDirect

International Journal of Electrical Power and Energy Systems

journal homepage: www.elsevier.com/locate/ijepes

Quantized deep learning model based Volt-Var control for hosting capacity maximization: a practical case study

Muhammad Kamran Khan [a,*], Kimmo Kauhaniemi [a], Hannu Laaksonen [a], Muhammad Hamza Zafar [b]

[a] School of Technology and Innovation, University of Vaasa, Finland
[b] Department of Engineering Sciences, University of Agder, Grimstad 4879, Norway

ARTICLE INFO

Keywords:
Hosting capacity (HC)
Modified Reptile search Algorithm (MRSA)
Quantized 1D Convolutional Neural Network (QCNN)
Decoupled Finite Control Set Model Predictive control (D-FCS-MPC)
Post-Training Quantization (PTQ)
and EN 50549 standard

ABSTRACT

This study introduces a data-driven Volt-Var control strategy aimed at maximizing hosting capacity (HC) and mitigating voltage violations in distribution networks. Central to the proposed methodology is a quantized one-dimensional convolutional neural network (QCNN), developed to emulate optimal Volt-Var control decisions. Post-training quantization is applied, resulting in tenfold reduction in model size, making QCNN well-suited for deployment on resource-constrained edge devices. The training data is prepared using Modified Reptile Search Algorithm, which determines optimal Volt-Var control set points for HC maximization. The QCNN model trained offline processes measurements from the test network to predict the optimal reactive power reference points, which are supplied to the Decoupled Finite Control Set Model Predictive Controller (D-FCS-MPC). The D-FCS-MPC subsequently determines the optimal inverter switching states to directly regulate reactive powers to the predicted reference values. The methodology is validated using model of a real-world medium voltage (MV) network situated in Vaasa, Finland, known as the Sundom Smart Grid (SSG). Both simulation and OPAL-RT based real time results confirms the effectiveness of the proposed methodology in maximizing hosting capacity and ensuring grid stability.

1. Introduction

The increasing penetration of renewable energy sources like PV and wind generation presents significant challenges related to the power system stability and managing hosting capacity (HC) [1]. A report submitted by Clean Energy Group in May 2023 points out that about 429 MW of energy storage and 2,321 MW of PV capacity are stuck in interconnection queues in Massachusetts [2].The reason being the limiting HC of the existing grid. Also, Yle News report that continued development of large-scale solar farms in eastern Finland could create bottlenecks in the FINGRID transmission network. These challenges demand a systematic evaluation of the grid known as hosting capacity analysis.

Regulators and distributed system operators (DSOs) are particularly interested in determining the extent to which the current power systems can handle the future generation and demand without violating system limits. HC is defined as "the total DER capacity that can be accommodated on a given feeder without adversely impacting reliability and stability of the grid" [3]. The HC of a network is usually limited by frequency fluctuations, power quality issues, voltage limits, thermal limits and protection measures [4]. Thermal overloading and overvoltage are the most crucial factors that limits the HC of a distribution network. DERs are connected to the grid through smart inverters (SIs). These SIs, equipped with efficient control functions, offers an efficient solution for increasing the HC of distribution networks [5,6].

Numerous methods have been studied in the literature to evaluate and improve the distribution network hosting capacity [7–9].In [10], a Differential Evolution (DE) optimizer was explored to identify the optimal placement, sizing, and power factor (pf) of DERs, with the primary goals of minimizing network losses and maximizing DER penetration. Similarly, the study in [11] employed a modified Particle Swarm Optimization algorithm to determine optimal power factor settings for preventing voltage violations in a real-world feeder. Volt-Var (Q(V)) control is one of the most widely used SI control modes for mitigating voltage violations and maximizing hosting capacity (HC) in distribution networks [12–14]. In [15], a Particle Swarm Optimizer was employed to

* Corresponding author.
E-mail address: kamran.khan@uwasa.fi (M.K. Khan).

https://doi.org/10.1016/j.ijepes.2025.111524
Received 18 March 2025; Received in revised form 15 December 2025; Accepted 21 December 2025
Available online 6 January 2026

Table 1
Summary of Recent Data-Driven Volt–Var Control Studies.

Ref.	Objective	Test Network	ML Technique	Grid code	Quantization
[30]	Voltage regulation	Real distribution feeder	Mean-Corrected Recursive Ridge Regression	IEEE 1547	No
[31]	Voltage regulation	Real distribution feeder	Deep Reinforcement Learning	–	No
[34]	Voltage regulation	IEEE 33-bus	Constrained Temporal Convolutional Network	–	No
[36]	Voltage regulation	IEEE 33 & 123 bus system	Deep Convolutional Neural Network	–	No
[37]	Voltage regulation	IEEE 123-bus	Deep Neural Network	–	No
[38]	Voltage regulation Loss minimization	IEEE 33-bus system	Multi-Agent Soft Actor Critic	–	No
[32]	Voltage regulation Loss minimization	IEEE 33-bus system	Deep Convolutional Neural Network	IEEE 1547	No
[34]	Voltage regulation Loss minimization	IEEE 33-bus system	Constrained Temporal Convolutional networks	–	No
This study	HC maximization Voltage regulation	Real distribution feeder	Deep Convolutional Neural Network	EN 50549	Yes

optimize the location, size, and Volt-Var control set-points for distributed energy resources in a medium voltage distribution feeder. The algorithm effectively mitigate overvoltage issues, leading to a 32.1 % increase in HC. In reference [16], the problem of maximizing hosting capacity and minimizing voltage deviations was formulated as a multi-objective nonlinear optimization and solved using the Slime Mould Algorithm. This approach determined the optimal locations, sizes, and Volt-Var Control based power dispatch for photovoltaic and battery energy storage systems. In [17], the Equilibrium Optimization Algorithm was employed to optimize the locations, sizes, and Volt-Var control settings, with the goal of maximize the hosting capacity of the IEEE 123-bus test system.

Since DERs are connected to the distribution grid via three-phase inverters, an efficient control technique is crucial for optimally regulating inverter switching and managing active and reactive power set-points within the grid [18,19]. Successful implementation of model predictive control-based Volt-Var control has been reported in few research articles[20–22]. In [23], a Volt-Var control strategy was developed using Model Predictive Control (MPC) and compared against a traditional PID controller. The results demonstrated the superior performance of the MPC controller in maximizing the hosting capacity of an IEEE-9 bus test system. The research in [24] investigated PI controller-based Volt-Var, Volt-Watt and Volt-Var-Watt control schemes for maximizing the HC in a distribution network.

In recent years, supervised deep learning techniques have garnered significant attention from researchers [25,26]. These methods leverage large datasets and advanced machine learning architectures to accurately model complex, nonlinear relationships between voltage and reactive power [27–29]. In [30], a data-driven distributed energy resource management system (DERMS) was introduced for voltage regulation. Unlike traditional approaches, the method eliminates reliance on detailed network models by leveraging real-time grid and DER measurements to determine optimal dispatch strategies, while simultaneously minimizing active power curtailment. Furthermore, in [31], a reinforcement learning framework employing the Importance Weighted Actor-Learner Architecture (IMPALA) was proposed for Volt-VAR and PQ optimization in solar-powered distribution grids.

In [32], a data-driven deep convolution neural network was designed and trained to generate optimal local voltage control curves. The effectiveness of the proposed method was validated using an IEEE 33 bus test system. In [33], an ANN controller was trained to replicate the optimal centralized control set points of a photovoltaic (PV) inverter in a decentralized manner, using data optimized by chance constraint optimal power flow. Reference [34] proposed a data-driven Volt-Var Control strategy using Constrained Temporal Convolutional Networks (C-TCN) to reduce power losses and mitigate voltage violations. The C-TCN model incorporates a corrective layer to penalize constraint violations and was validated on the IEEE 33-bus system. The study in [35] employed a Multilayer Perceptron (MLP) to manage the active and reactive power setpoints of DERs, with the objective of minimizing power losses and maintaining the voltage profile within acceptable limits. Table 1 presents a comparison of various data-driven Volt–Var control strategies for smart inverters in distribution networks.

Contributions

Most existing studies rely on conventional Volt-Var control methods, such as those specified in IEEE 1547, often neglecting critical factors like the nonlinearity of Volt-Var curves, deadband ranges, and the complexity of real-world grid scenarios. This oversight leads to suboptimal performance. Moreover, a notable research gap exists in the development of advanced control strategies tailored to optimize DER integration while ensuring compliance with modern grid codes. In comparison to the existing research, the major contributions of this study are:

- Detailed HC analysis of a real-world MV network situated in Vaasa, Finland, known as the Sundom Smart Grid (SSG).
- A Modified Reptile Search Algorithm (MRSA) is proposed to determine optimal size, location, dynamic deadband ranges, and Volt-Var slopes for maximizing hosting capacity.
- A novel data-driven volt-var control for HC maximization is proposed, in which a quantized 1D convolutional neural network (QCNN) model is developed to emulate Volt-Var control. Trained on historical load and generation data from the Sundom Grid, the deep learning model effectively captures the complex nonlinear relationships between voltage and reactive power.
- Post-training quantization is applied to reduce model size for real-world deployment. Quantization results in a tenfold reduction in model size, making QCNN well-suited for deployment on resource-constrained edge devices like microcontrollers.
- A novel control framework is investigated, where the D-FCS-MPC tracks the power setpoints predicted by the deep learning model. The control framework is verified using OPAL-RT–based real-time simulator. Under various DER penetration scenarios, the D-FCS-MPC controller gives a smooth and robust control response within the allowed tolerance levels mentioned in EN 50549–2 grid codes.

The paper is divided into 5 sections. The mathematical modelling of the proposed Volt-Var control strategy and optimization problem formulation for HC maximization is presented in section 2. Section 3 explains in detail the research methodology. Finally, sections 4 and 5 presents the results and discussions.

2. Standards and methods

This section gives a brief introduction of EN 50549 grid codes and explains in detail the mathematical modelling of the Volt-Var control. Furthermore, this section also explains the formulation of HC maximization as an optimization problem.

2.1. Grid codes

Grid codes describe the operational and technical requirements of the equipment to be connected to the power system. Compliance with grid codes ensures that the equipment willing to connect will not harm

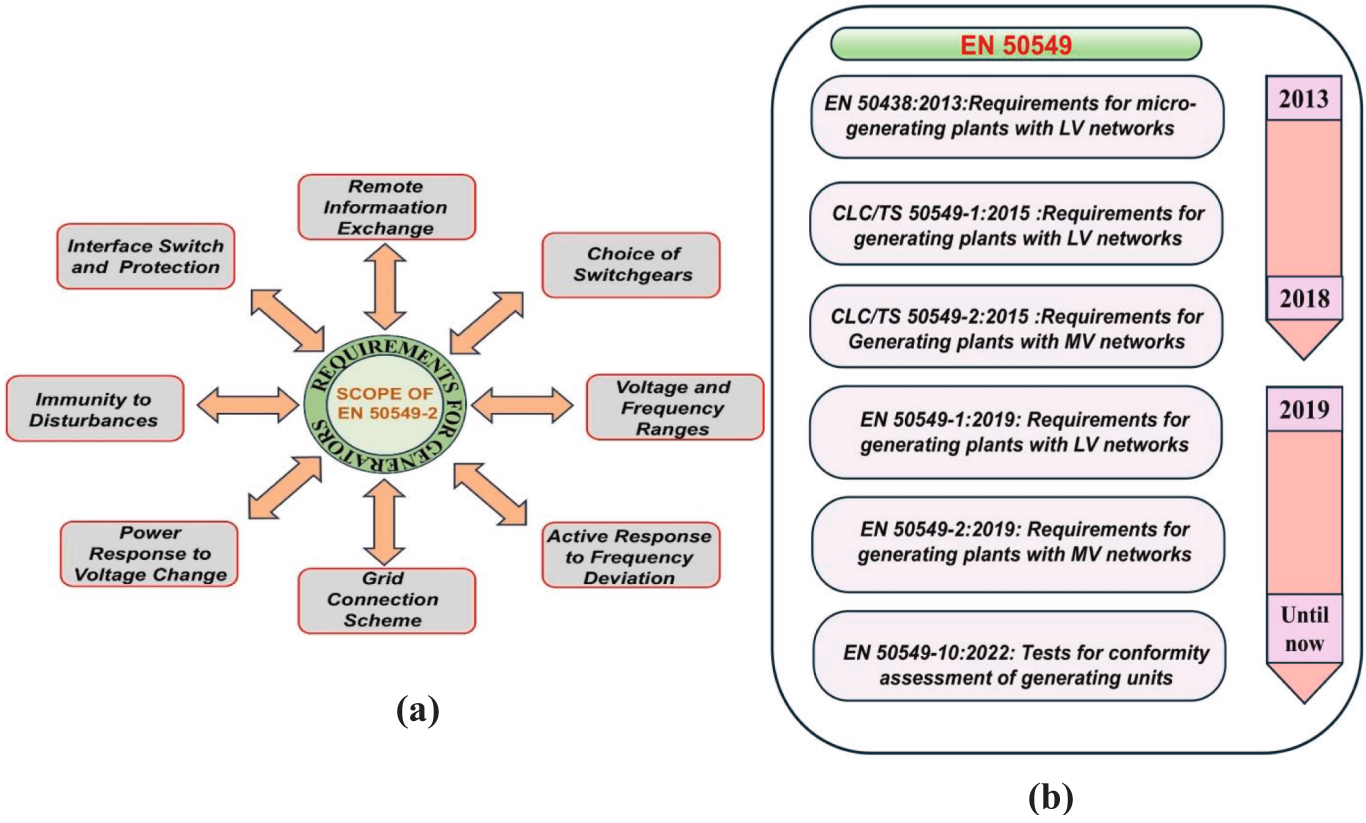

Fig. 1. (a) Scope of EN 50549 (b) Evolution of EN 50549 standard.

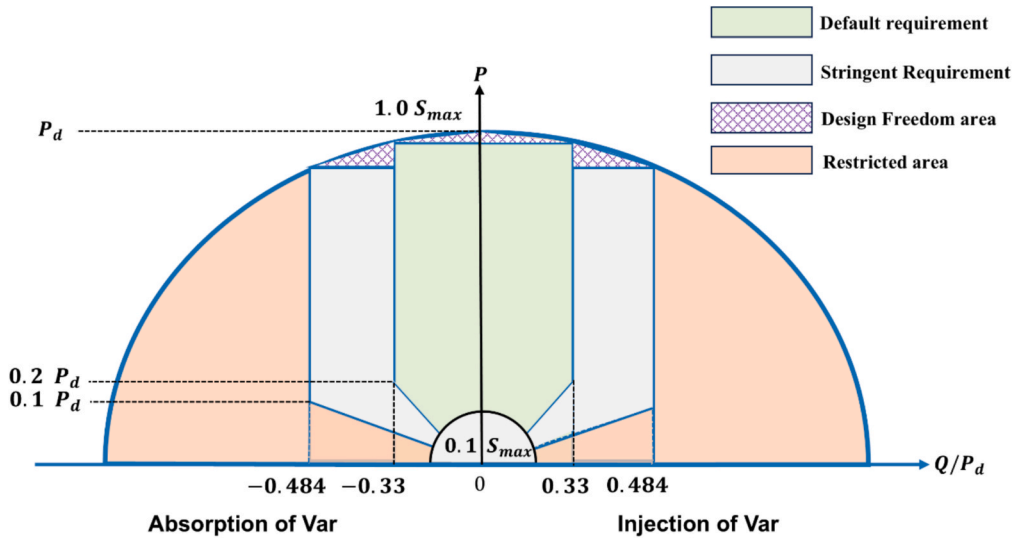

Fig. 2. Required Reactive Power Capability according to EN 50549.

stability and reliability of the grid. EN 50549 grid codes, published by the European Committee for Electrotechnical Standardization (CENELEC), have been widely adopted across Europe. These Standards relate to both the RfG European Network Code requirements and current technical market needs. Fig. 1 illustrates the structure and development of the EN 50549 series.

2.1.1. Voltage support by reactive power

Modern grid codes demand various ancillary services from the grid connected DER units such as regulating reactive and/or real power to keep the voltage at PoC within the acceptable limits. According to EN 50549–2 the acceptable voltage ranges from 90 % to 110 % of the nominal voltage. The default requirements mentioned in EN 50549–2 are as follows:

- The reactive power requirement for Q is up to 33 % of the demanded active power (P_d) over-excited and under-excited when P is above 20 %P_d.

Table 2
SI control modes.

Modes	STANDARDS FINGRID VJV 2018 [39]	IEEE 1547 [40]	California Rule-21 [41]	EN 50,549 [42]	
Q(V)	✓	✓	✓*	✓	
Q setpoint	✓*	✓	–		✓*
Q(P)	–	✓	✓	✓	
P(V)	–	✓	–	✓	
CosΦ setpoint	✓	✓*	✓	✓	
Cos Φ(P)	–	–	–	✓	

* : Default mode.

- If active power is less than 20 % of P_d, the DER unit should be capable of injecting or absorbing reactive power up to a minimum pf of 0.52 as shown in Fig. 2.
- The stringent requirements reactive power requirement is up to 48.4 % of P_d over-excited and under-excited, when P exceeds 20 % of P_d.
- When operating below 20 % of P_d the reactive power shall be provided according to Fig. 2 with a minimum pf of 0.38.

2.2. Modelling of SI control

Distributed energy resources (DERs), such as photovoltaic systems or wind turbines, are typically connected to the grid via smart inverters (SIs). These SIs can actively participate in grid management by injecting or absorbing reactive power. Table 2 outlines different SI control modes defined in various standards.

2.2.1. Volt-Var control

In Volt-Var (Q(V)) control mode, the inverter dynamically regulates the reactive power (Q) based on the measured voltage at the point of connection (v_m) as illustrated in Fig. 3. The proposed Volt-Var control introduces static (fixed) and dynamic (variable) dead bands (dB) to accommodate different voltage ranges. If v_m falls between dynamic and static dB ranges, the inverter does not provide any reactive power support. The static dB is nonadjustable and ranges from 0.95 pu to 1.05 pu. In contrast, the limits of the dynamic dB are adjustable, with the upper limit v_{du} ranging from 1.05 pu to 1.099 pu, and the lower limit v_{dl} from 0.9 pu to 0.95 pu. The length of the dynamic dB can be adjusted to get the maximum value of HC. In this study the optimal length of the dynamic dead band is determined by selecting v_{du} and v_{dl}, with the aim of maximizing hosting capacity (HC).

When the measured voltage (v_m) exceeds the upper dynamic dB limit (v_{du}), the inverter behaves as an inductor and absorbs Q. Alternatively, when $v_m < v_{dl}$, inverter injects reactive power. Furthermore, the rate of reactive power injection/absorption is dependent on the slope (m) of the Q(V) curve. By determining the optimal values of Volt-Var slopes (m) and dynamic dead band limits (v_{du}, v_{dl}), SIs can efficiently manage reactive power absorption/injection to maximize hosting capacity. Based on these ideas, the reactive power as a function of measured voltage, dynamic dead band voltage limits, and slope is mathematically formulated as:

$$Q_{DER} = P_d * \begin{cases} \beta(|v_m - v_{du}|)\, m_u, if v_m > v_{du} \\ \beta(|v_m - v_{dl}|) m_l, if v_m < v_{dl} \\ \beta * 0.484, if v_u > v_m > v_l \\ 0, if v_{dl} < v_m < v_{du} \end{cases} \tag{1}$$

$$m_{u,l} = \frac{Q_{max} - Q_{min}}{v_{u,l} - v_{du,dl}} \tag{2}$$

$$\beta = \frac{v_r - v_m}{|v_r - v_m|} \tag{3}$$

Here, $v_r = 1$ and P_d is the demanded active power. The value of β can be either -1 or 1. The positive β implies reactive power injection while negative value means reactive power absorption.

2.2.2. Optimization problem

The problem is defined as a constraint, non-convex and nonlinear optimization problem. The objective is distribution network HC maximization.

$$\underset{d}{Max} \sum_{g=1}^{N_{DER}} P_{DER,g}^{inst} \tag{4}$$

Here, $d = [N, S_{DER}, m_u, m_l, v_{du}, v_{dl}]^T$ is a decision vector which includes location (N), size (S_{DER}) and Volt-Var control setpoints (slopes (m) and dead band limits (v_d)).N_{DER} = number of buses containing DERs. The load flow constraints are represented in equations (5) and (6).

$$P^G + P_k^{DER} - P_k^d = |V_k| \sum_{n=1}^{N_b} |V_n| (G_{kn} cos\theta_{kn} + B_{kn} sin\theta_{kn}) \tag{5}$$

$$Q^G + Q_k^{DER} - Q_k^d = |V_k| \sum_{n=1}^{N_b} |V_n| (G_{kn} sin\theta_{kn} + B_{kn} cos\theta_{kn}) \tag{6}$$

Here, P^g and Q^g show grid active and reactive powers; P_k^{DER} and Q_k^{DER}

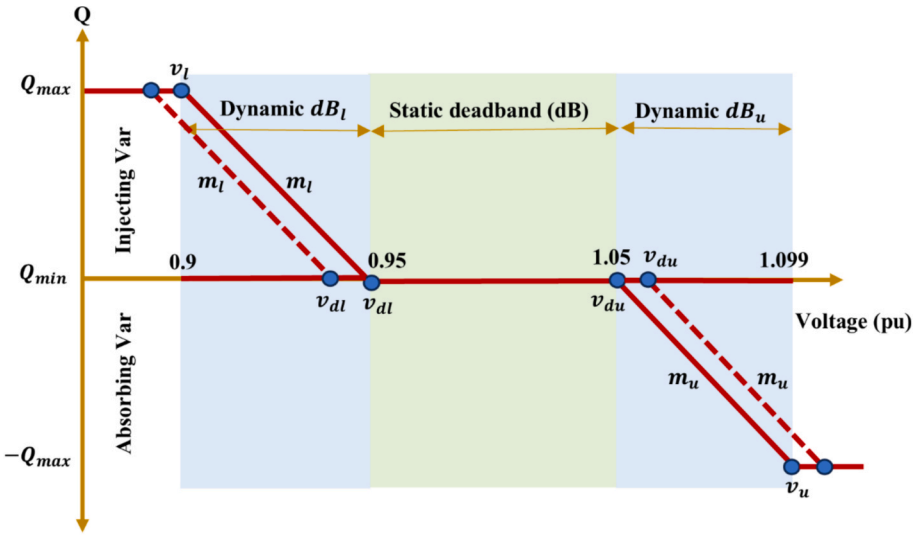

Fig. 3. Volt-Var curve.

represent active and reactive power generation at bus k while P_k^d and Q_k^d are the demanded active and reactive powers at bus k; N_b = total number of buses; V_k and V_n are bus k and n voltages; G_{kn} and B_{kn} represents real and imaginary part of bus admittance matrix; θ_{kn}= angle difference between bus k and n.

$$V^{min} \leq V_k \leq V^{max} \qquad \forall k \in N_b \tag{7}$$

$$I_{kn} \leq I_{kn}^{rated} \qquad \forall k \in N_b \tag{8}$$

$$S_{DER}{}^{min} \leq S_{DG,k} \leq S_{DER}{}^{max} \qquad \forall k \in N_{DER} \tag{9}$$

$$m^{min} \leq m_k^{u,l} \leq m^{max} \qquad \forall k \in N_{DER} \tag{10}$$

$$v_d{}^{min} \leq v_{d_k}^{u,l} \leq v_d{}^{max} \qquad \forall k \in N_{DER} \tag{11}$$

The equations (7), (8) and (9) modeled the voltage, current and DER installed capacity constraints. Furthermore, the minimum and maximum slope and dynamic dead band limits are given by equations (10) and (11) respectively.

3. Methodology

This study introduces a data-driven Volt-Var control strategy aimed at maximizing hosting capacity (HC) and mitigating voltage violations in distribution networks. Central to the proposed methodology is a quantized one-dimensional convolutional neural network (QCNN), developed to emulate optimal Volt-Var control decisions. For dataset preparation, a Modified Reptile Search Algorithm (MRSA) is employed to determine optimal reactive power setpoints for HC maximization. The prepared dataset is used to train the QCNN, enabling it to predict optimal reactive power reference points based on real-time measurements from the test network. These reference points are subsequently provided to a Model Predictive Control (MPC) framework, which calculates the optimal inverter switching states to directly regulate reactive powers to the predicted reference values. Therefore, the methodology of this research is organized into three sections. Section 3.1 introduces the modified reptile search algorithm (MRSA) and explains how it can be applied to determine optimal size and location of DER along with SI control set points for hosting capacity maximization in a distribution network. Section 3.2 focuses on the quantized one-dimensional convolution network, detailing its use in data driven volt var control. Finally, Section 3.3 explains the decoupled Finite Control Set Model Predictive Control (D-FCS-MPC) framework, for precise active and reactive power control in the network.

3.1. Modified reptile search algorithm

The reptile search algorithm (RSA), a metaheuristic approach, consists of two main stages: the encircling stage and the hunting stage.

3.1.1. Encircling stage as exploration

The encircling phase involves exploring the search space. In the encircling phase, crocodile movements are mathematically modelled as:

$$x_{mn}(i+1) = best_n(i)\left(-\mu_{(mn)}(i)\right) \times \beta - \left(R_{(mn)}(i) \times rand\right), i \leq \frac{T}{4} \tag{12}$$

$$x_{mn}(i+1) = best_n(i) \times x_{(r_1,n)} \times ES(i) \times rand, i \leq 2\frac{T}{4} and\ i > \frac{T}{4} \tag{13}$$

Where,

$$\mu_{(mn)} = best_n(i) \times P_{(mn)} \tag{14}$$

$$R_{(mn)} = \frac{best_n(i) - P_{(r_2,n)}}{best_n(i) + \epsilon} \tag{15}$$

x_{mn} represent n_{th} position of the m_{th} solution,$Best_n(i)$ represent optimal solution, rand represent random number between 0 and 1, i and T show current and maximum iterations.

3.1.2. Hunting stage as exploitation

The encircling involves exploiting the search space and consist of hunting coordination and cooperation, which are mathematically modelled as:

$$x(mn)(i+1) = best_n(i) \times (P_{(mn)}(i)) \times rand, i \leq 3\frac{T}{4} and\ i > 2\frac{T}{4} \tag{16}$$

$$x(mn)(i+1) = best_n(i) - \mu_{(mn)}(i) \times \epsilon - R_{(mn)}(i) \times rand, i \leq T\ and\ i > 3\frac{T}{4} \tag{17}$$

where, $best_n(i)$ is the best solution in the current iteration. The detailed explanation of these equations can be found in [43].

3.1.3. Proposed modified reptile search algorithm (MRSA)

When addressing the high dimensional, nonlinear and non-convex HC maximization problem, the original RSA exhibits prominent shortcomings, such as local maxima stagnation, inadequate convergence and high computational complexity. To overcome these issues, some modifications are introduced in the original algorithm.

a) Cosine operator in the exploration phase

The main cause of local maxima trapping is inadequate exploration during the high walking stage. To improve exploration, a cosine operator is introduced in the encircling phase. The addition of cosine function enhances the exploration of the search space in the initial stages and prevent trapping in the local maxima. With the inclusion of cosine operator, Eq. (12) is replaced by the following equation:

$$x_{mn}(i+1) = best_n(i) + (r_1 \times cos(rand) \times |r_2 \times best_n(i) - x_{mn}|, for\ i \leq \frac{T}{3} \tag{18}$$

Here $rand$, r_1 and r_2 are the random numbers.

b) Levy flight in the exploitation phase

The second modification is designed to improve the convergence during the hunting phase of the original RSA. To achieve this, the Levy operator is used, which includes a jump size control factor, denoted by ξ:

$$levy = 0.01 * \frac{u}{v^{\frac{1}{\xi}}} \tag{19}$$

where, v and u follows the normal distribution.

$$u\ N\left(0, \sigma_u^2\right), v\ N(0, \sigma_v^2) \tag{20}$$

$$\sigma_u = \left(\frac{\lambda(1+\xi) sin\frac{\pi\xi}{2}}{\lambda\left[\frac{1+\xi}{2}\right] \xi * 2^{\frac{\xi-1}{2}}} \right)^{1/\xi} \tag{21}$$

$$\sigma_v = 1 \tag{22}$$

λ represents the gamma function, while ξ is a crucial parameter that controls the jump size of the search particles. A smaller value of ξ results in shorter, random steps during the exploitation phase, enabling solution candidates to effectively explore the vicinity of the current best solution. This improves the algorithm's ability to achieve global convergence. Therefore, equation (17) is replaced with the following equation in the modified algorithm:

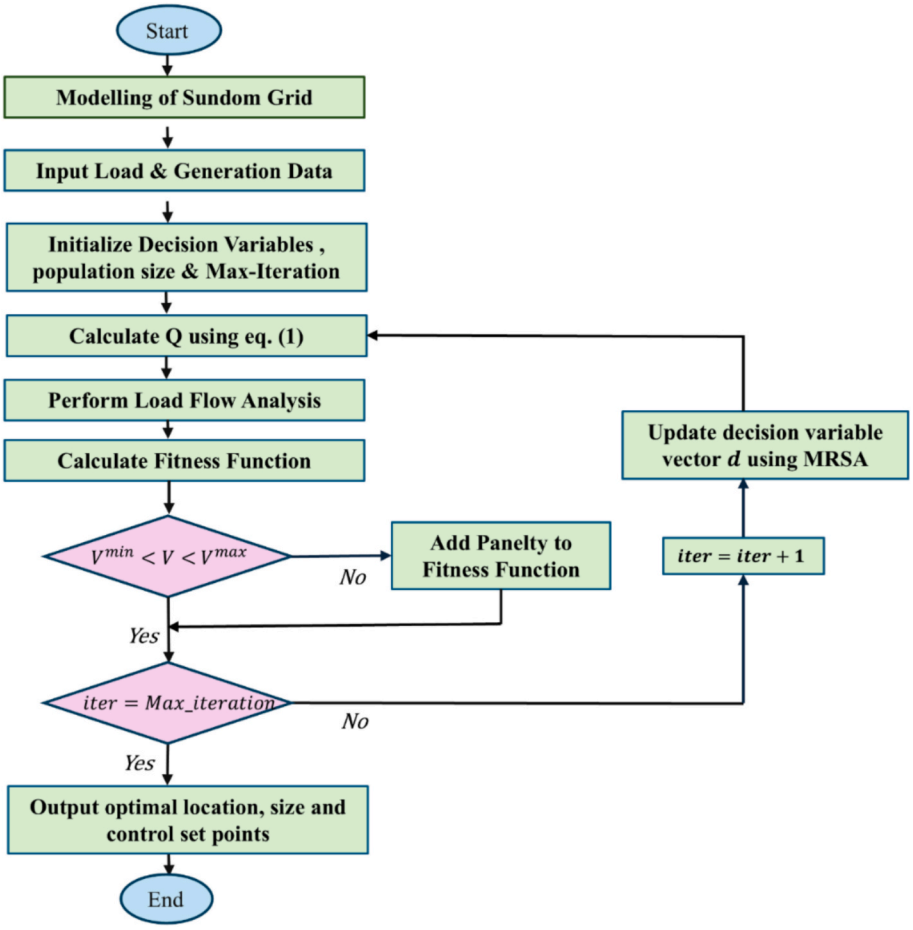

Fig. 4. MRSA based HC maximization methodology.

$$x_{mn}(i+1) = best_n(i) + rand \times levy \times (x_{mn} - best_n(i)), for\ i \le T\ and\ i > 3\frac{T}{4} \tag{23}$$

In the original algorithm, equations (14) & (15) are computationally intensive, leading to increased time complexity. However, with the aforementioned modifications, these equations no longer need to be calculated in MRSA algorithm, resulting in a 2-to-3-fold reduction in time complexity.

3.1.4. MRSA for HC maximization

The methodology of maximizing hosting capacity using the MRSA algorithm is illustrated by a flowchart in Fig. 4. The procedure begins with modeling the distribution network. Next, the MRSA parameters are initialized, including the population size and dimensions, sensitivity

Table 3
Methodology of Data Driven Volt Var control.

Algorithm: Proposed data driven Volt-Var control-based HC maximization
Step 1: *Collect historic load and generation data of the test network (Sundom Grid)*
Step 2: *Apply k-means clustering to reduce the number of scenarios (n).*
Step 3: *Data set preparation*
for *k = 1: n*
Determine optimal control set points using MRSA optimizer (explained in section 3.1.4)
Calculate optimal Q using equation (1)
end
Load prepared dataset to the neural network
Step 4: *Training and validation*
Reshape the data for 1 D CNN
Split the data into training and testing samples
Build a 1D CNN with multiple layers and initialize weight and biases.
Train the deep learning model and calculate loss function
Calculate outputs using trained 1D CNN
Save the offline trained model
Step 5: *Post-training quantization*
Apply quantization to the pretrained model
Calculate outputs using quantized 1D CNN (QCNN)
Save the quantized deep learning model
Step 6: *Implement the pre-trained deep learning model for HC maximization.*

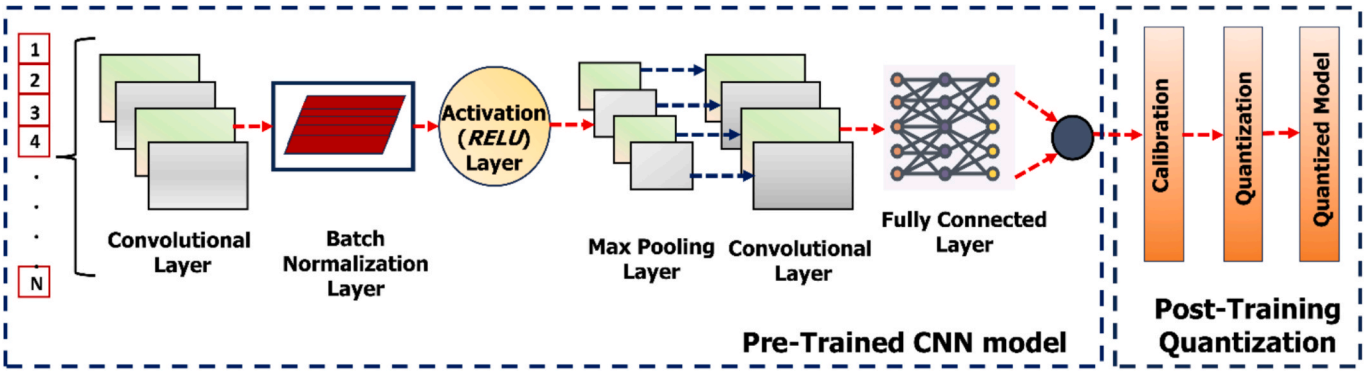

Fig. 5. Structure of Quantized 1D CNN model (QCNN).

parameter (β), sensitivity limit (α), jump size (ξ), maximum iterations (T), and iteration counter (*i*). The population consists of a decision variable vector *d*, which includes the slope of the Volt-Var curve (*m*), length of the upper dynamic dead band (v_{du}), the location (*N*) and size of the DER (*S*).

After initialization, the fitness function is evaluated, and the decision vector (*d*) that yields the maximum hosting capacity value (objective function) is chosen. If any operational constraint is violated, a penalty is applied to the cost function, reducing the fitness function value to zero. Afterwards, MRSA updated the decision vector for the next iteration, and the fitness function is evaluated for the updated values. The entire process is repeated for the predefined number of iterations. Once the stopping criteria is met, the decision vector with the optimal cost function value (active power) is selected as the final output.

3.2. Proposed data driven Volt Var control

Applying data-driven Volt-VAR control for hosting capacity maximization involves leveraging real-time and historical data to optimize voltage and reactive power management in a power distribution network. The summary of the proposed data driven volt var control-based HC maximization process is presented in Table 3.

3.2.1. Data set preparation

The initial step involves collecting hourly averaged historical load and generation data from the test network over a one-year period. The collected data contains numerous scenarios that can be overwhelming, potentially leading to computational inefficiencies. To address this, k-means clustering is applied to reduce the dataset to manageable number of representative scenarios. After clustering a data set is prepared considering each representative scenario. In this dataset, load, generation, and voltage values are used as input features. The corresponding optimal reactive power, determined using the MRSA optimization algorithm with the objective of maximizing HC, is designated as the target output.

3.2.2. One-Dimensional convolutional neural network (1D CNN)

A 1D CNN is a variant of convolutional neural network designed to process one-dimensional sequential data. It consists of convolutional layers with filters that slide over the input sequence, performing dot products at each position to produce feature maps. The convolution operation for a 1D CNN can be mathematically represented as:

$$y_k = ((x^{*}w) + b) = \sum_{i=0}^{l-1} (x(k+i).w(i)) + b \tag{24}$$

where * represent the discrete convolution operation; *x* is the input signals,*w* represent filter of length *l* and *k* is the filter position, while *b* represent the bias parameter. After the convolution operation, the feature maps are passed through the ReLU activation function, defined as follows:

$$y_k = ReLU(y_k) = max(0, y_k) \tag{25}$$

The ReLU is preferred because it introduces nonlinearity which allows the model to capture complex patterns in the data. Additionally, the ReLU function also helps to avoid the vanishing gradient problem by maintaining stronger gradients. The output is then passed through a pooling layer. Pooling (e.g., max pooling) is a down sampling operation that reduces the size of the output:

$$y_{pole} = max_{j=0}^{p-1}(y_{k.p+j}) \tag{26}$$

Where *p* is the pooling size. The cost function (loss function) which needs to be minimized during the training process is defined as ridge regularized normalized root mean square error between true and predicted reactive power (Q):

$$f_{loss} = \sqrt{\frac{\sum_{j=1}^{N}(Q_j - \overline{Q_j})^2}{N} + \lambda \sum_{k=1}^{m}(w_k)^2} \tag{27}$$

Here Q_j and $\overline{Q_j}$ are the true and predicted reactive power values; N is the total number of samples and w_k represents weights of the model. The second term represent a ridge regularization process which prevent overfitting by adding a penalty to the model coefficients. In this work, regularization strength (λ) of 0.01 is utilized. 1D CNN is used because it automatically learn local patterns in the data by applying convolutional filters, making it highly effective at detecting important features [44]. This reduces the need for manual feature engineering and often results in improved performance compared to traditional regression models.

3.2.3. Quantization

Quantization is a powerful technique for deployment of DL models on resource-constrained edge devices [45]. Quantization maps 32-bit floating-point model parameters to an 8-bit representation. This reduction in precision decreases model size, accelerates inference, and reduces power consumption. The quantization function can be formulated as follows [46]:

$$Q(r) = Int(\frac{r}{S}) - Z \tag{28}$$

where *Int* is a function that maps a real valued input *r* to an integer value by using a rounding operation, *S* represent scaling factor, and *Z* is the zero-point offset. In this study both weights and activations of 1D CNN model were quantized using the post-training quantization (PTQ), resulting in a reduction in model size with approximately no loss in accuracy. The structure of Quantized 1 D CNN is presented in Fig. 5.

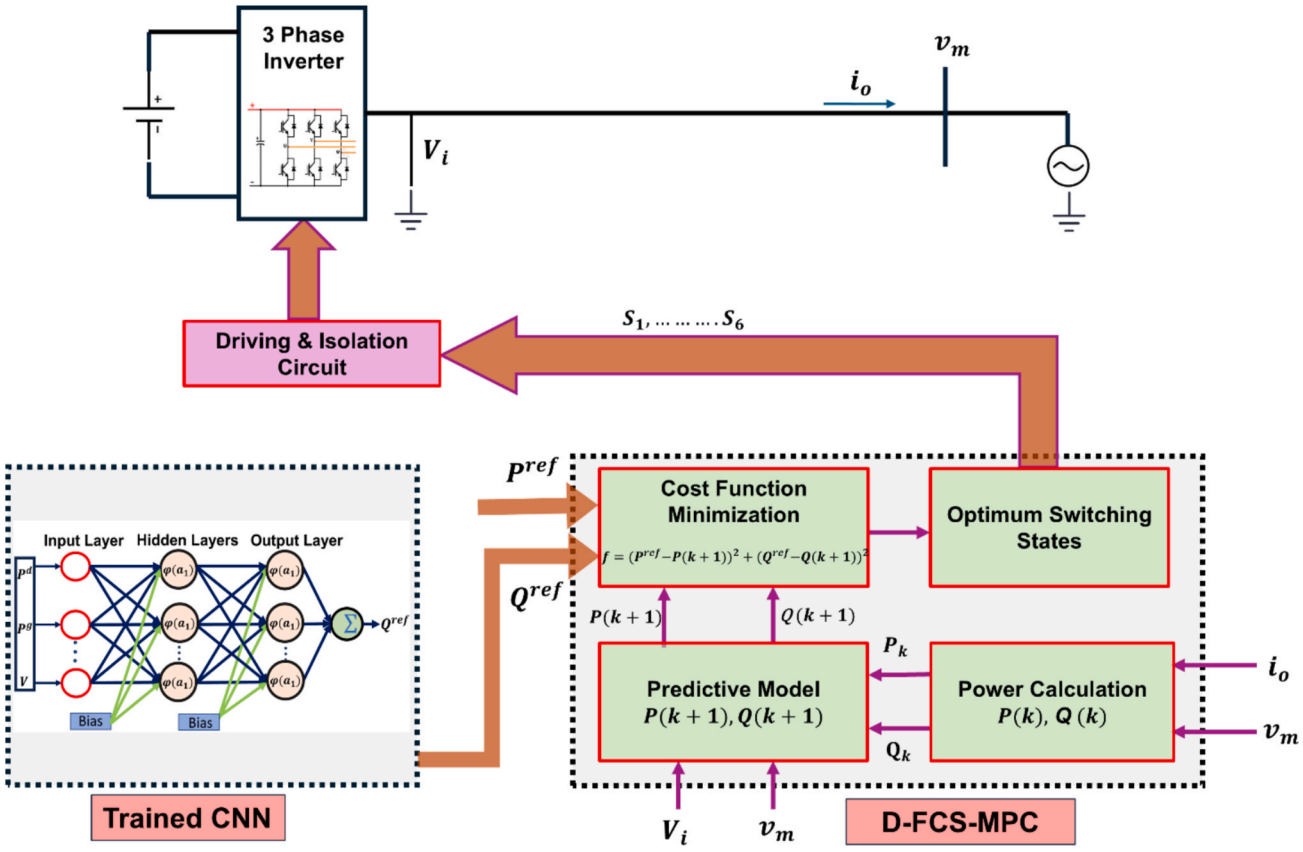

Fig. 6. Proposed D-FCS_MPC based control with pre-trained deep neural network.

3.3. D_FCS_MPC based controller with 1D CNN

The methodology of the decoupled finite control set model predictive control (D-FCS-MPC) combined with a deep convolutional network is illustrated in Fig. 6. A pre-trained deep learning model (as explained in section 3.2 of methodology) processes measurements from the test network to predict the optimal reactive power reference points, which are then supplied to the MPC controller. The MPC controller subsequently determines the optimal inverter switching states to directly regulate both active and reactive powers to meet the provided reference values.

3.3.1. Decoupled Finite control set model Predictive control (D-FCS-MPC)

FCS-MPC is a specialized form of MPC designed to handle systems with discrete control actions. D-FCS-MPC regulate active and reactive powers directly, without the need for intermediate control loops, enabling fast, simplified, and decoupled control [47]. D-FCS-MPC provide robust and efficient discrete control and can be utilized to control switch states of grid tied inverters [48]. D-FCS-MPC control for 3 phase grid tie inverters consist of three steps:

(a) **Measuring current states:** The first step involves developing a mathematical model that captures the current states of the system. For the implementation of D-FCS-MPC, an inverter model is developed using P and Q as state variables. Equation that calculates the current active and reactive power is:

$$x(j) = \begin{bmatrix} P \\ Q \end{bmatrix} = \frac{3}{2} \begin{bmatrix} v_{m,\alpha} & v_{m,\beta} \\ v_{m,\beta} & -v_{m,\alpha} \end{bmatrix} \begin{bmatrix} i_{o,\alpha} \\ i_{o,\beta} \end{bmatrix} \tag{29}$$

Here, $x(j) = [P\ \ Q]^T$ is the state variable at the current sampling instant k, $v_m = \begin{bmatrix} v_{m,\alpha} & v_{m,\beta} \end{bmatrix}^T$ is the voltage measured at the point of connection and, $i_o = \begin{bmatrix} i_{o,\alpha} & i_{o,\beta} \end{bmatrix}^T$ is the line current.

(b) **Creating a prediction model:** This step involves creating a prediction model to estimate future behavior of the system over a defined time horizon (t_s). The prediction model is formulated as,

$$x(j+1) = x(j) + \left[Ax(j) + \frac{3}{2L} BV_i(j) - \frac{3}{2L} Cv_m(j) \right] t_s \tag{30}$$

Here,

$$A = \begin{bmatrix} -\frac{R}{L} & -\omega \\ \omega & -\frac{R}{L} \end{bmatrix} \tag{31}$$

$$B = \begin{bmatrix} v_{m,\alpha} & v_{m,\beta} \\ v_{m,\beta} & -v_{m,\alpha} \end{bmatrix} \tag{32}$$

$$C = \begin{bmatrix} v_{m,\alpha} & v_{m,\beta} \\ 0 & 0 \end{bmatrix} \tag{33}$$

Here t_s = sampling time, $V_i = \begin{bmatrix} V_{i,\alpha} & V_{i,\beta} \end{bmatrix}^T$ is the inverter voltage and ω is the angular frequency. Equation (30) predicts the behavior of P and Q (state variables) in terms of inverter voltage space vector (V_i), grid voltage (v_m) vector and line current (i_o).

(c) **Minimizing Cost function:** In the third step, optimal space vectors for next sampling interval is identified to minimize the defined cost function. In this study the objective is optimal real and reactive power injection for HC maximization. Therefore, cost function L is:

$$L = (P^{ref} - P(k+1))^2 + (Q^{ref} - Q(k+1))^2 \tag{34}$$

Here, P^{ref} and Q^{ref} represent reference real and reactive powers provided by the deep learning model, while $P(k+1)$ and $Q(k+1)$

represent predicted real and reactive powers. To match predicted and desired reference powers, the control algorithm determines optimal space vectors for each sampling interval, thus minimizing the power error.

4. Test results

The results section is divided into four subsections for clarity and detailed analysis. Section 4.1 explains the test network. Section 4.2 evaluates the performance of the Modified Reptile Search Algorithm (MRSA) for HC computation by focusing exclusively on worst case scenario. Section 4.3 demonstrates the application of MRSA in generating a dataset that is subsequently used to assess the proposed data-driven Volt-Var Control approach (explained in section 3.2). Finally, Section 4.4 analyzes the effectiveness of the Decoupled Model Predictive Control (D-FCS-MPC) framework which calculates the optimal inverter switching states to directly regulate reactive powers to the predicted references provided by the trained neural network.

4.1. Test network

The test network used to evaluate the proposed methodology is a real-world MV network situated in Vaasa, Finland, known as the Sundom Smart Grid (SSG). The single-line diagram of Sundom Grid is shown in Fig. 8, with specific details provided in Table 4. The SSG, equipped with intelligent electronic devices (IEDs), functioned as a pilot laboratory in collaboration with the University of Vaasa. The SSG supported various research activities through data collection and real-time communication. A cloud service gathered IEC 61850 sampled values and Generic Object-Oriented Substation Event (GOOSE) measurements from various points across the grid. For this study, hourly average load and generation data measured over the course of one year is utilized as illustrated in Fig. 7.

Table 4
Test network specifications.

Test Network	Details
No. of metering units	2500 (Small commercial and residential users)
Wind generation	3.6 MW
Feeders	4
Feeder Length	J6 Sulva: 7.93 km (C) + 25.24 km (O) = 33.182 km J7 Sundom: 10.19 km (C) + 12.95 km (O) = 23.141 km J8 Wind: 0.733 km (C) J9 Vaskiluoto: 1.12 km (C) + 5.91 km (O) = 7.03 km
Conductors	Sparrow AF40, AHXW 3x95, AL 132, Raven AF62, AHXW 185, Swan AF25, SAX-W 50

*C: Underground Cable, *O: Overhead Line.

4.2. Hosting capacity

The performance of the Modified Reptile Search Algorithm (MRSA) for HC computation was assessed through extensive simulations conducted using MATLAB software. The analysis focused on key grid metrics such as thermal loading and overvoltage. The HC evaluation was carried out under extreme operating conditions, specifically maximum generation and minimum load scenario. The load and DER generation values used in this analysis are marked by purple circles in Fig. 7.

The Sundom Grid comprises four feeders: J9 Vaskiluoto, J8 Wind, J7 Sundom, and J6 Sulva. Feeder J8 already hosts a 3.6 MW wind turbine, and no additional installations were considered for this feeder in the analysis. Feeder J9, a short feeder with a length of 7.035 km, was analyzed in detail. The analysis on J9 indicated that neither overvoltage nor thermal loading pose any limitations on the hosting capacity (HC). The focus is then shifted to feeders J6 and J7, where a detailed analysis revealed that overvoltage was the primary factor limiting DER hosting capacity. Additionally, the HC was found to be significantly influenced by the locations of DER installations. To address this, five potential installation sites were selected for each feeder, considering environmental, climatic, and topographical factors, as shown in Fig. 8.

Two cases were considered in this analysis:

Case 1: HC was evaluated using location and size of DER as decision variables, without employing any control.
Case 2: The Volt-Var (Q(V)) control was activated, and the optimal size, location, dynamic deadband limits and slopes were identified to maximize hosting capacity.

Each test case involved evaluating multiple scenarios to determine grid level and feeder level hosting capacity by using MRSA algorithm. For feeder J7, Scenarios 1 and 4 examined the effects of installing one and two DER units, respectively. Similarly, Scenario 2 and 5 analyzed the installation of one and two DER units on feeder J6. In the grid-wide HC analysis, Scenario 3 considered installing one DER unit on both feeders J6 and J7, while Scenario 6 evaluated two DER units on each feeder. In all scenarios, the minimum DER installation was fixed at 2 MW. Also, for scenarios with one DER unit, the maximum installation

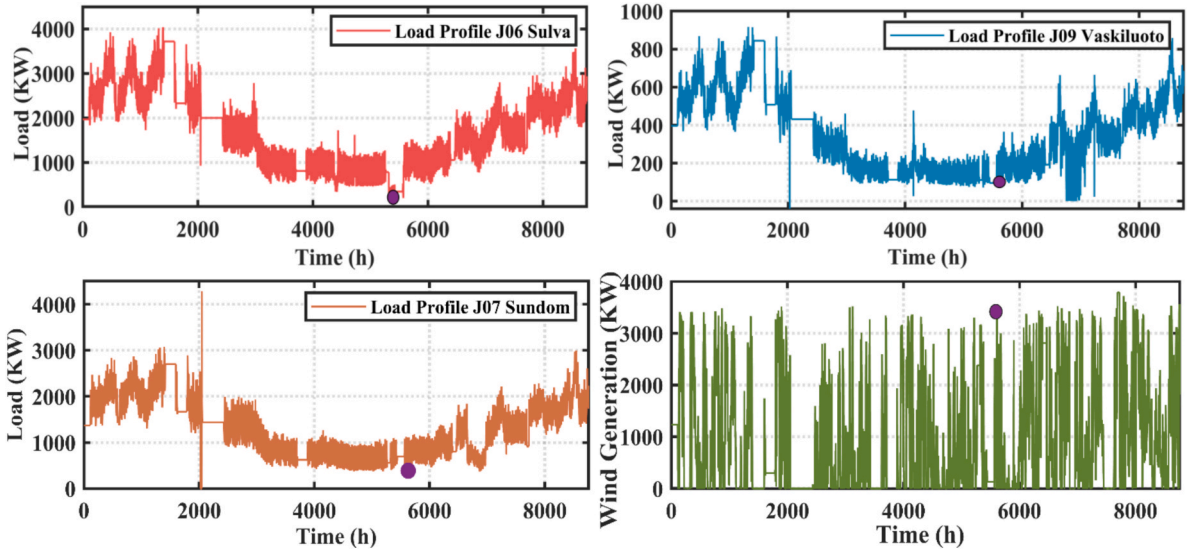

Fig. 7. Sundom Grid hourly load and generation data for one year.

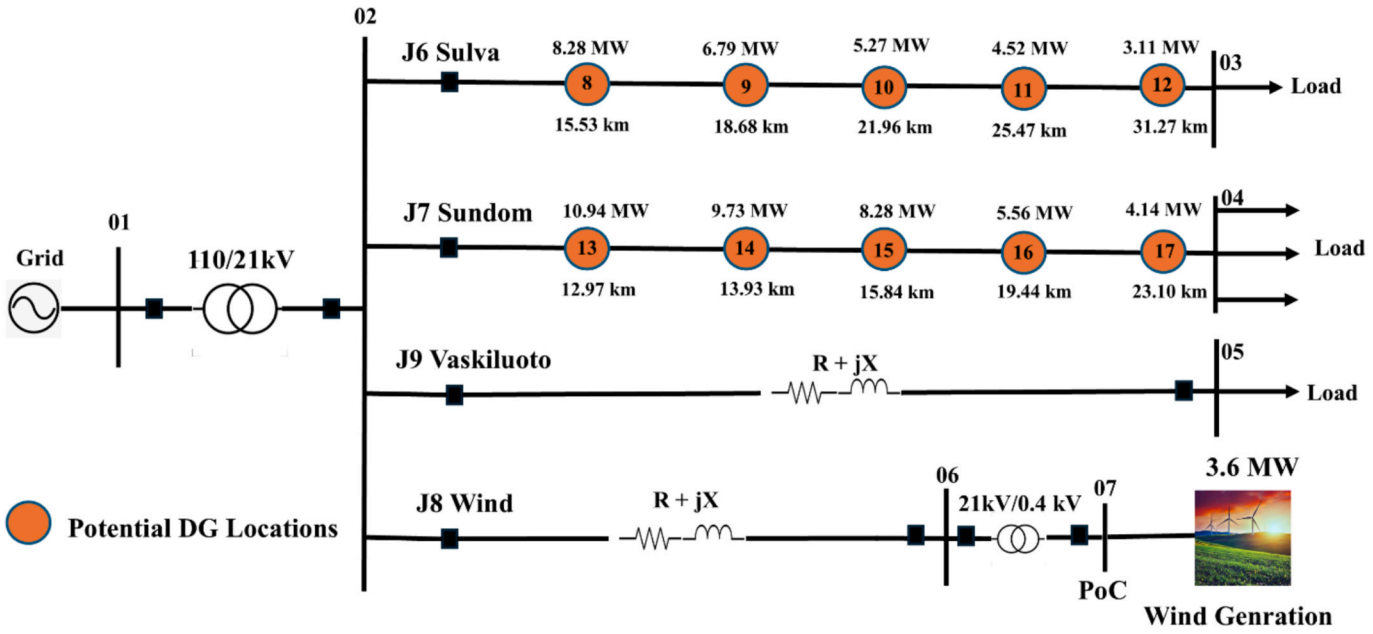

Fig. 8. Sundom Grid with potential locations and HC values.

was limited to 16 MW, while for scenarios with two DER installation, it was reduced to 8 MW per unit. The simulation parameters are presented in Table 5.

For case 1, the results in Table 6 indicate that the highest hosting capacity of 18.784 MW was achieved by simultaneous installation of two DER units, one with a capacity of 10.783 MW on feeder J7 and another with a capacity of 8.001 MW on feeder J6.On feeder J7, the HC reached 10.942 MW when a single DER unit was installed at the 13th location, while for feeder J6, the HC was 8.2881 MW with a DER installed at the 8th location. Similarly, when two DER units were installed at optimal locations, the achieved HC values on Feeders 6 and 7 were 10.561 MW and 7.330 MW, respectively.

Table 7 presents the hosting capacity (HC) values when Volt-Var (Q (V)) control is applied. The results showed that with Volt-Var control, the maximum HC increased from 18.784 MW to 27.368 MW in Scenario 3, representing a 45.858 % increase compared to the no-control case (case 1). On feeder J7, an HC value of 13.818 MW was achieved by installing a single DER at location 13, while a HC of 12.989 MW was obtained by installing two DER units at locations 13 and 14. Similarly, for feeder J6, HC values of 9.827 MW and 8.559 MW were achieved in Scenarios 2 and 5, respectively. In all cases, the results indicate that higher HC values are attained by placing a single DER unit at the optimal location, rather than deploying multiple DER units along the feeder. The Volt-Var curves for various locations are presented in Fig. 9.

Comparative Analysis: The performance of the proposed MRSA algorithm is evaluated against various state-of-the-art metaheuristic algorithms, including the traditional Reptile Search Algorithm (RSA), Grasshopper Optimization Algorithm (GOA) [49], and Particle Swarm Optimization (PSO) algorithms [50]. The convergence curves for various considered scenarios are presented in Fig. 10. The results clearly show that MRSA achieves an average improvement of 0.49 % in HC

Table 5
Simulation settings.

Simulation Parameters	Values
Population	50
Max. iterations	50
Dynamic deadband range	1.05-1.099 pu
v_u^{max}	1.15 pu
Slope (k_u) range	4-48
α, β, ξ	0.8, 0.1, 0.01
Voltage threshold	1.1 pu
Installed DER range	2 MW – 16 MW

Table 6
Case 1 results: no control.

Scenarios	Feeder J7 Location/Size (MW) DER # 1	DER # 2	Feeder J6 Location/Size (MW) DER # 1	DER # 2	HC (MW)
1	13/10.942				10.942
2	–	–	8/ 8.281	–	8.2881
3	13/10.783	–	8/ 8.001	–	18.784
4	13/ 7.140	14/ 3.422	–	–	10.561
5	–	–	8/ 5.273	9/ 2.057	7.330
6	13/7.147	14/ 3.079	8/ 4.339	9/ 1.907	16.472

Table 7
Case 2 results: volt-var control.

Scenarios	Feeder J7 Location/ Size (MW)/ [v_{dBu}, *slope*] DER # 1	DER # 2	Feeder J6 Location/ Size (MW)/ [v_{dBu}, *slope*] DER # 1	DER # 2	HC (MW)
1	13/ 13.8181/ [1.080, 9.490]	–	–	–	13.8181
2	–	–	8/ 9.8272/ [1.087, 15.612]	–	9.8272
3	13/ 15.7281/ [1.056, 6.472]	–	8/ 11.64/ [1.062, 5.551]	–	27.3681
4	13/ 7.2522/ [1.059, 8.972]	14/ 5.7368/ [1.063, 7.111]	–	–	12.9890
5	–	–	8 / 6.3662/ [1.052, 8.689]	9 / 2.1930/ [1.073, 9.244]	8.5592
6	13/ 6.1357/ [1.091, 5.172]	15/ 3.233/ [1.058, 11.518]	8 / 6.7441/ [1.077, 12.745]	9 / 6.4586/ [1.069, 8.827]	22.5714

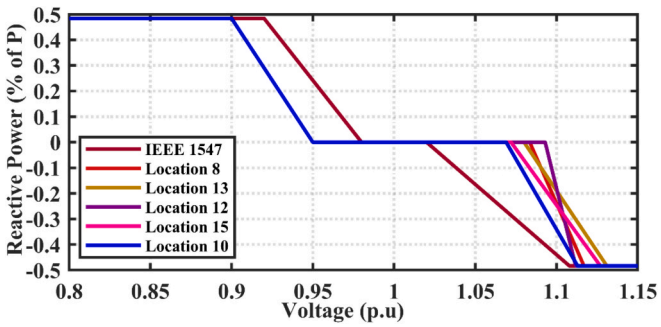

Fig. 9. Optimal linear Volt-Var curves determined by MRSA algorithm.

value compared to the PSO algorithm and outperforms other algorithms in terms of global optima search capability. Furthermore, to ensure a fair evaluation, each algorithm was executed 15 times, and the results are presented using a box plot in Fig. 11. These findings highlight that the modified RSA, enhanced through strategic improvisations, demonstrates robust global optimization capabilities, consistently surpassing other algorithms in terms of precision, reliability, and overall effectiveness.

4.3. Performance evaluation of data driven Volt-Var control

This section evaluates the performance of the proposed data driven volt var control for the Sundom grid. The analysis utilizes data from the summer season, specifically between 3000 and 6000 h, which represents lower load and higher generation scenarios. Real-world data, as shown in Fig. 7, contains numerous scenarios that can be overwhelming, potentially leading to computational inefficiencies. To address this, k-

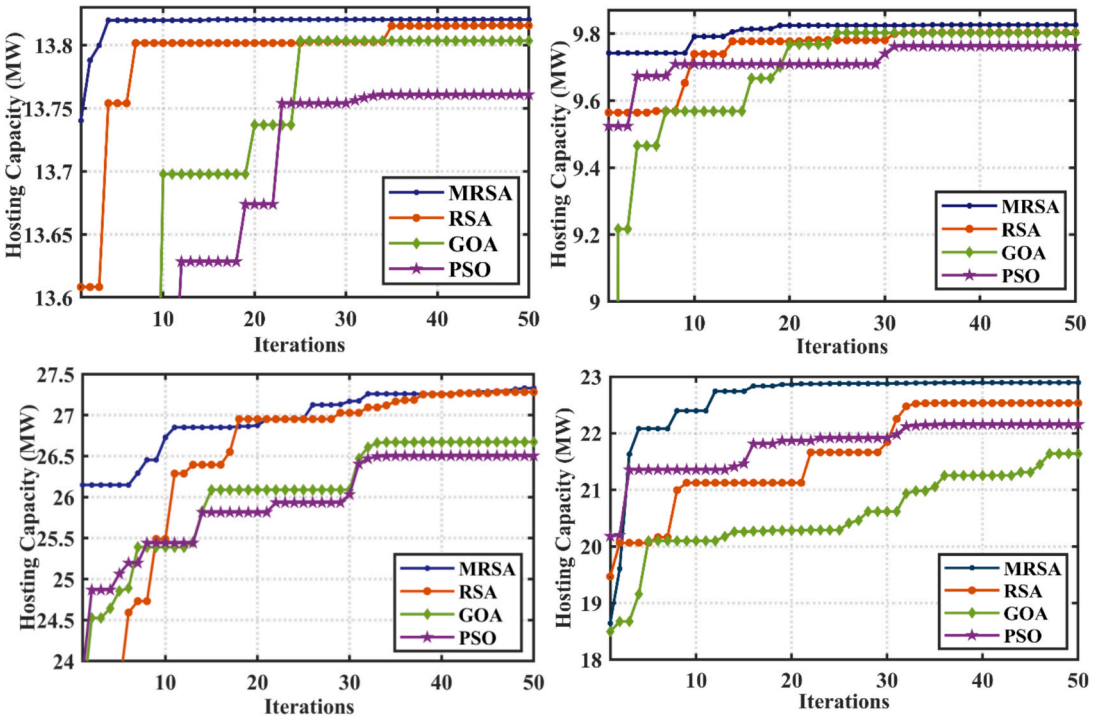

Fig. 10. Convergence Curves for scenarios 1, 2, 3 and 6.

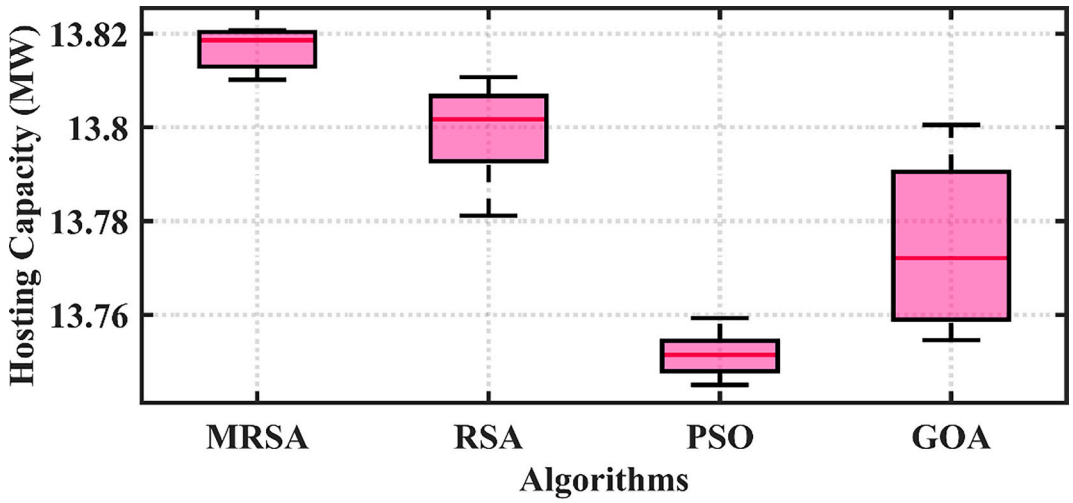

Fig. 11. Box Plot of various algorithms.

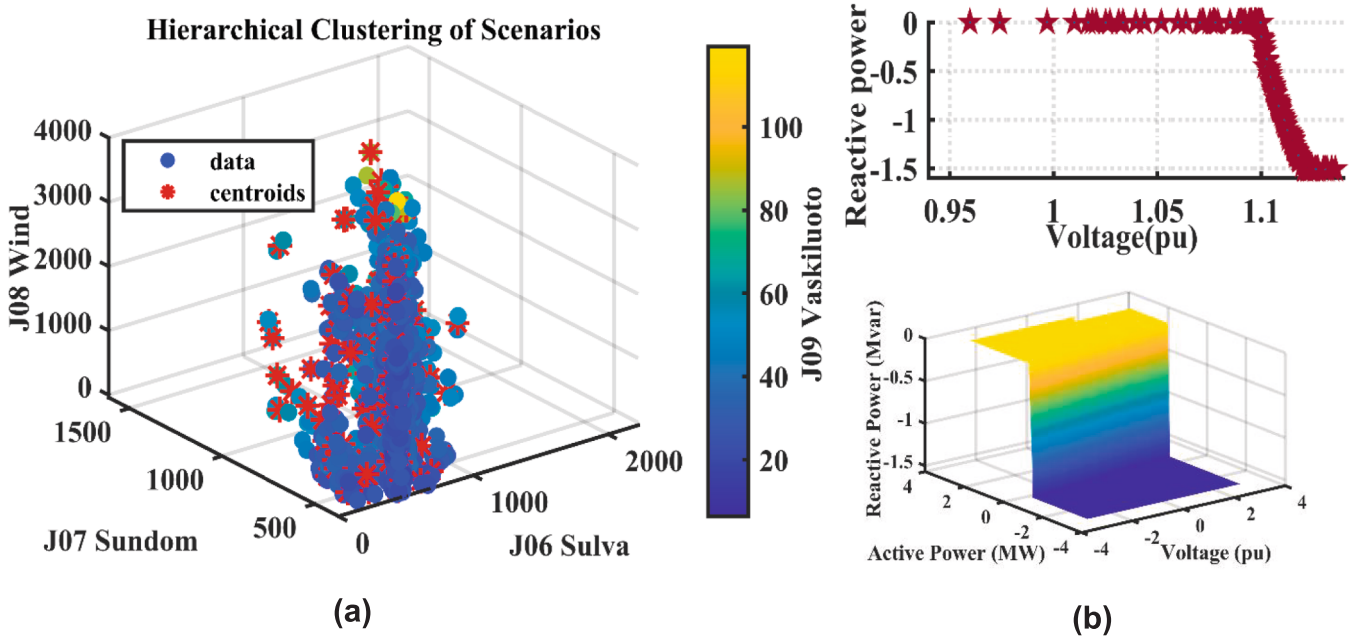

Fig. 12. Data set preparation (a) clustering of scenarios (b) Data driven Volt-Var curves.

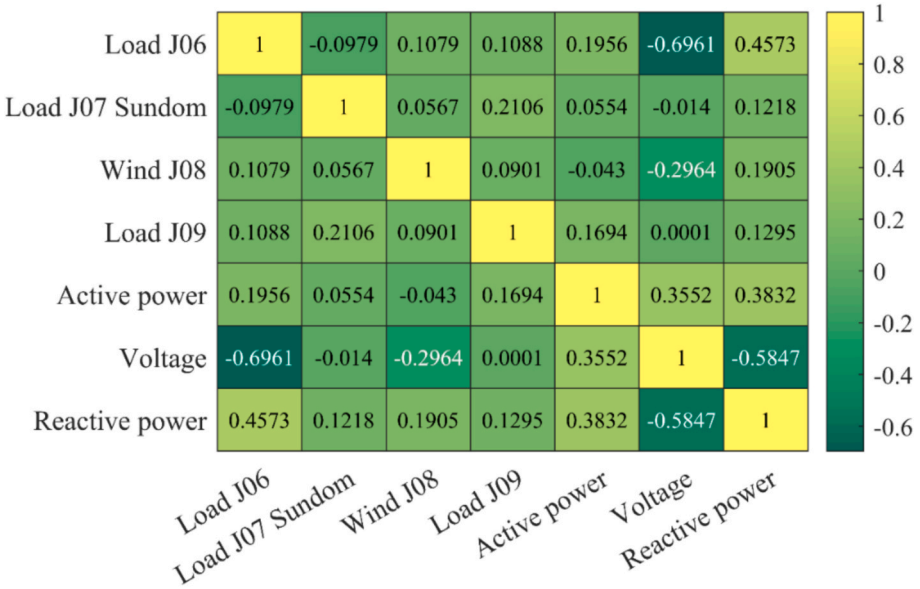

Fig. 13. Correlation matrix of the dataset.

means clustering is applied to reduce representative scenarios. The clustering streamline the dataset while preserving the diversity and representativeness of the original data. Additionally, to enhance the quality of the data set, some randomly generated scenarios were also added by intuition.

After clustering, a dataset is prepared with load, generation, and voltage as inputs, and reactive power as the output. The dataset is created considering a single DER installation at bus 03 of feeder J6 Sulva. For each scenario, the optimal reactive power output is determined using the MRSA optimization algorithm. The data-driven 2D and 3D Volt-Var curves constructed from the prepared dataset are shown in Fig. 12 (b). The 2D curves reveal that the Volt-Var curves generated from real-world load and generation scenarios exhibit nonlinear behavior, in contrast to the conventional linear Volt-Var curves depicted in Fig. 9.

The correlation analysis of the dataset is shown in Fig. 13. The correlation matrix indicates a strong correlation between the load on feeder J6, voltage, and reactive power, as well as a moderate positive correlation between active generation and reactive power output. There is significant multicollinearity between J6 load, voltage and reactive power which can lead to overfitting. This overfitting issue is addressed by applying L2-regularization in the cost function. A multilayered quantized 1D CNN model containing three convolutional layers is utilized for prediction. The model is trained for 50 epochs with a batch size of 32, using the Adam optimizer. Additionally, the dataset is split into three parts: 80 % for training, 10 % for validation, and 10 % for testing.

The prediction results for both the quantized and non-quantized 1D CNN models are presented in Fig. 14. The results demonstrate that the predicted values closely align with the true values, indicating a high level of accuracy in the trained model. Furthermore, the performance of the quantized model is identical to the non-quantized model, showing

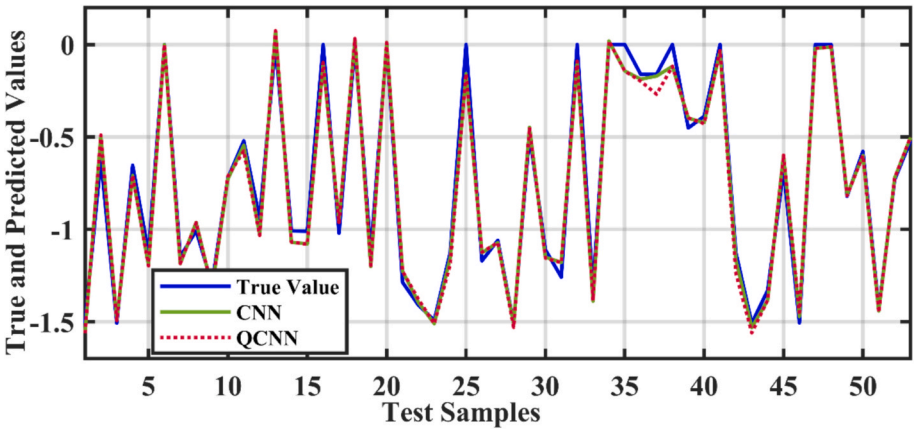

Fig. 14. Prediction results of quantized and non-quantized 1-DCNN models.

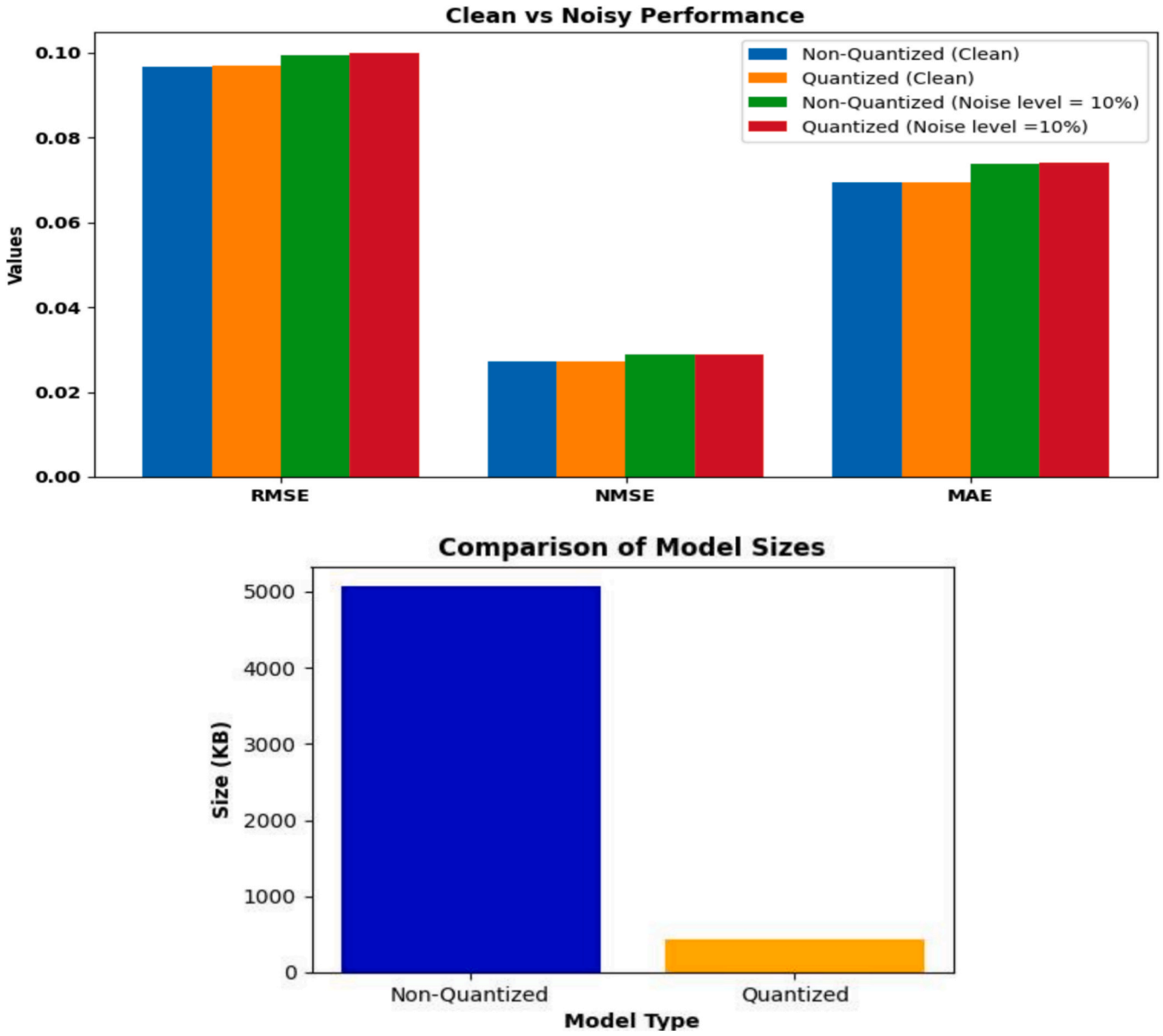

Fig. 15. Comparative analysis of performance metrics for quantized and non-quantized CNN models.

Table 8
Comparison of Performance Metrics.

Model Type	RMSE	NMSE	MAE	Size (KB)
Non-Quantized	0.09672133	0.0271639	0.0692889	5071.85
Quantized	0.09684882	0.0272356	0.0693220	439.91
Non-Quantized (Noise)	0.09924032	0.0288751	0.0738533	5071.85
Quantized (Noise)	0.09981813	0.0288899	0.0739615	439.91

that quantization did not significantly affect accuracy. Furthermore, the efficiency of the trained models is evaluated using various performance indices, including normalize mean square error (NMSE), root mean square error (RMSE) and mean absolute error (MAE), as shown in Fig. 15 and summarized in Table 8. The results indicate a 10-fold reduction in model size for the quantized version, with only a negligible loss in accuracy, demonstrating the effectiveness of quantization in optimizing model performance.

Data-driven models often operate as "black boxes" and are inherently sensitive to measurement uncertainties, unforeseen operating conditions, and missing data. To mitigate these limitations, various multi-fidelity modeling approaches have been proposed in the literature [51,52], which aim to improve robustness by integrating data sources of varying accuracy. In this study, to specifically assess the robustness of the proposed data-driven model under noisy conditions, we introduce relative Gaussian noise into the dataset. The noisy dataset is generated using the following relation:

$$x\_noise = +\eta.x.N(0,1) \tag{35}$$

Herex_noise = data with noise, x = clean data, η = noise level (set to 10 %) and $N(0,1)$ is the normal random variable with zero mean and unit variance. As illustrated in Fig. 15, introducing 10 % relative Gaussian noise results in a slight increase in RMSE, NMSE, and MAE. However, the overall performance of both quantized and non-quantized models remains stable, thereby confirming the robustness of the proposed data-driven model against measurement uncertainties and validating its reliability under noisy conditions.

The model is first trained in an offline environment to develop the best control strategy. Once the deep learning model is fully trained, it is deployed within the Sundom Grid to manage reactive power and optimize grid performance in real-time. To assess the reactive power management capabilities of the trained neural network models, a subset of real-world Sundom Grid scenarios, spanning from 3400 to 5900 h, is used as input for both the quantized and non-quantized neural network models. The results are presented in Fig. 16. The results show that both CNN and QCNN effectively predict optimal reactive power setpoints under varying load and generation conditions during voltage violations. They successfully restore voltage to its normal operating ranges, thereby enhancing the network's hosting capacity (HC).

4.4. Performance evaluation of D-FCS-MPC based control with 1D CNN

This section evaluates the performance of the designed decoupled model predictive controller for optimal reactive power management. To carry out this evaluation, the considered Sundom grid test network was modeled in MATLAB Simulink. Simulations were performed under two operational modes: no control (NC) mode and data driven Volt-Var (Q(V)) control mode. In NC, no Volt-Var control is enabled while in case of Q(V) control pre-trained deep learning model (evaluated in section 4.3) processes measurements from the test network to predict the optimal reactive power points for HC maximization. Model Predictive Control (MPC) calculates the optimal inverter switching states to directly regulate reactive powers to the predicted references provided by the trained deep learning neural network model. The controller performance is evaluated based on a single DER installation at bus 03 of feeder J6. The operating conditions for the test cases considered are detailed in Table 9.

4.4.1. Case 1: Moderate operating conditions

Case 1 considers moderate load and DER penetration scenarios. The results of case 1 are presented in Fig. 17. Fig. 17 (a) illustrates the results when SI control is not activated, while Fig. 17 (b) shows the results when Volt Var (Q(V)) control is enabled. Initially, the DER generates 0.9 MW of active power (P), while the voltage at PoC is 1.033 pu. Keeping the load constant, DER penetration increased to 1.9 MW at t = 0.3 sec, resulting in a voltage rise to 1.086 pu. Since the voltage at PoC stays within the permissible limits, the predicted Q is zero as shown in Fig. 17 (b, ii).

At t = 0.6 sec, the DER penetration increases to 2.956 MW, resulting

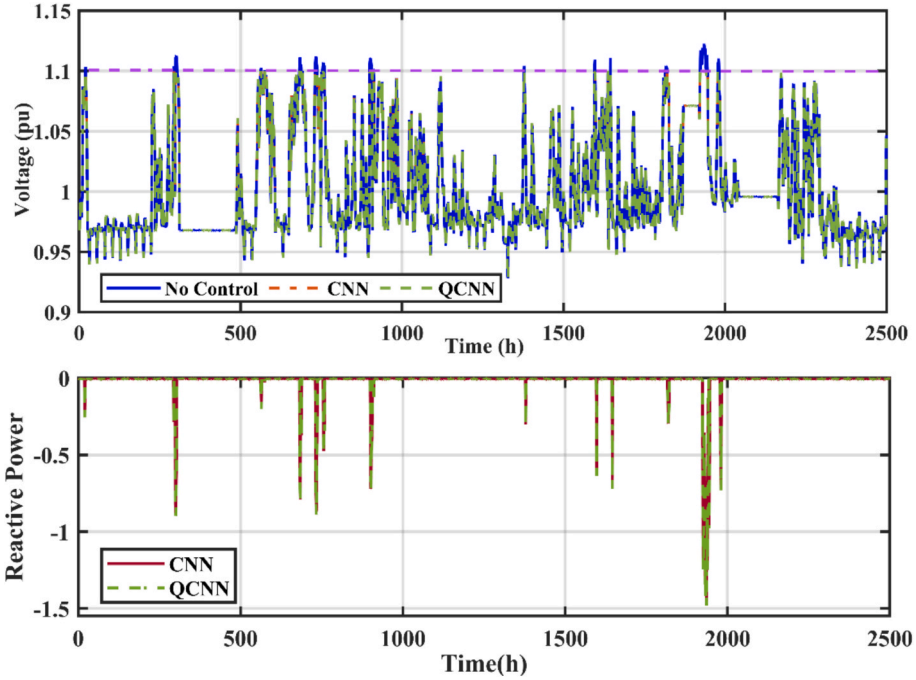

Fig. 16. Performance evaluation of CNN and QCNN models using subset of Sundom Grid scenarios.

Table 9
Operating conditions for case 1& 2.

Cases	Load J6 (MW)	Load J7 (MW)	Wind J8 (MW)	Load J9 (MW)	DER Generation (MW)
Case 1	0.652	0.5	3.6	0.033	2.956
Case 2	0.475	1.1318	3.6	0.033	3.0136

in a voltage rise to 1.1135 pu as shown in Fig. 17 (a, iii). When Volt-Var control is disabled, no reactive power support is provided (Q = 0) as shown in Fig. 17 (a, ii). Therefore, the voltage remains at 1.135 pu resulting in voltage violations and limiting the HC at PoC. However, with the activation of SI control, the data driven Volt-Var control responds by absorbing 1.13 MVar of reactive power as illustrated in Fig. 17 (b, ii). This reactive power absorption restore the voltage to 1.099 pu (Fig. 17 (b, iii), effectively enhancing the HC limits at PoC.

4.4.2. Case 2: Extreme operating conditions

In case 2, extreme operating conditions i.e. minimum loading and maximum DER penetrations are considered to generate overvoltage conditions. As the DER penetration increases to 100 % (3.0136 MW) at t = 0.6 sec, the voltage at PoC increase to 1.122 pu resulting in an overvoltage scenario as illustrated in Fig. 18 (a, iii). However, when Volt-Var control is enabled, the controller absorbs 1.49 MVar of reactive power which brings the voltage back in the continuous operating range as depicted in Fig. 18 (b, ii) and Fig. 18 (b, iii).

4.4.3. OPAL -RT-based real-time verification

In this section, the OP4510 real-time simulator is integrated with MATLAB/ Simulink model to perform software in the loop (SIL) testing. In the SIL testing, both the plant model and the control algorithm run inside OPAL-RT, without any external hardware controller [53]. In comparison to traditional simulation, SIL provide higher fidelity validation by testing actual VHDL, C, or C++ codes that will eventually run on the embedded hardware[54]. SIL testing provide efficient verification of controller performance in a realistic real-time execution environment.

The MATLAB results (presented in 4.4.1 and 4.4.2) are validated using OPAL-RT-4510, a real time digital simulator which is equipped with Xilinx Kintex-7 FPGA technology. The hardware setup is presented in Fig. 19. The RT Lab simulator operates in hardware synchronization mode and transmit signals to the Keysight Infinium EXR058A Oscilloscope via the analog ports of the OP4510. The results obtained, as shown in Figs. 20 and 21, provide real-time validation of the simulated model, confirming its performance in conditions that closely resemble real-world operations.

The MATLAB results are validated using the OPAL-RT OP4510, a real-time digital simulator equipped with a Xilinx Kintex-7 FPGA and a quad-core CPU. The corresponding hardware setup is shown in Fig. 19. This setup demonstrates the OPAL-RT–based real-time platform used to validate the proposed controller. OPAL-RT executes Simulink models in real time through the RT-Lab software environment, where the model is divided into two subsystems: SM and SC. The SM (Simulation Master) subsystem contains the main model for real-time execution, while the SC (Simulation Console) subsystem includes scopes and console blocks for monitoring and user interaction. Communication between SM and SC is managed through OpComm blocks. In this study, the simulator is operated in hardware synchronization mode, transmitting signals to a Keysight Infinium EXR058A oscilloscope via OP4510′s analog ports. These ports are accessed using the OpCtrl block, which provides an interface to OPAL-RT I/O cards and supports up to 256 I/O lines. In this configuration, OpCtrl is set to control a TE0741 board, and the Analog Out block is employed to route the outputs to the first three analog

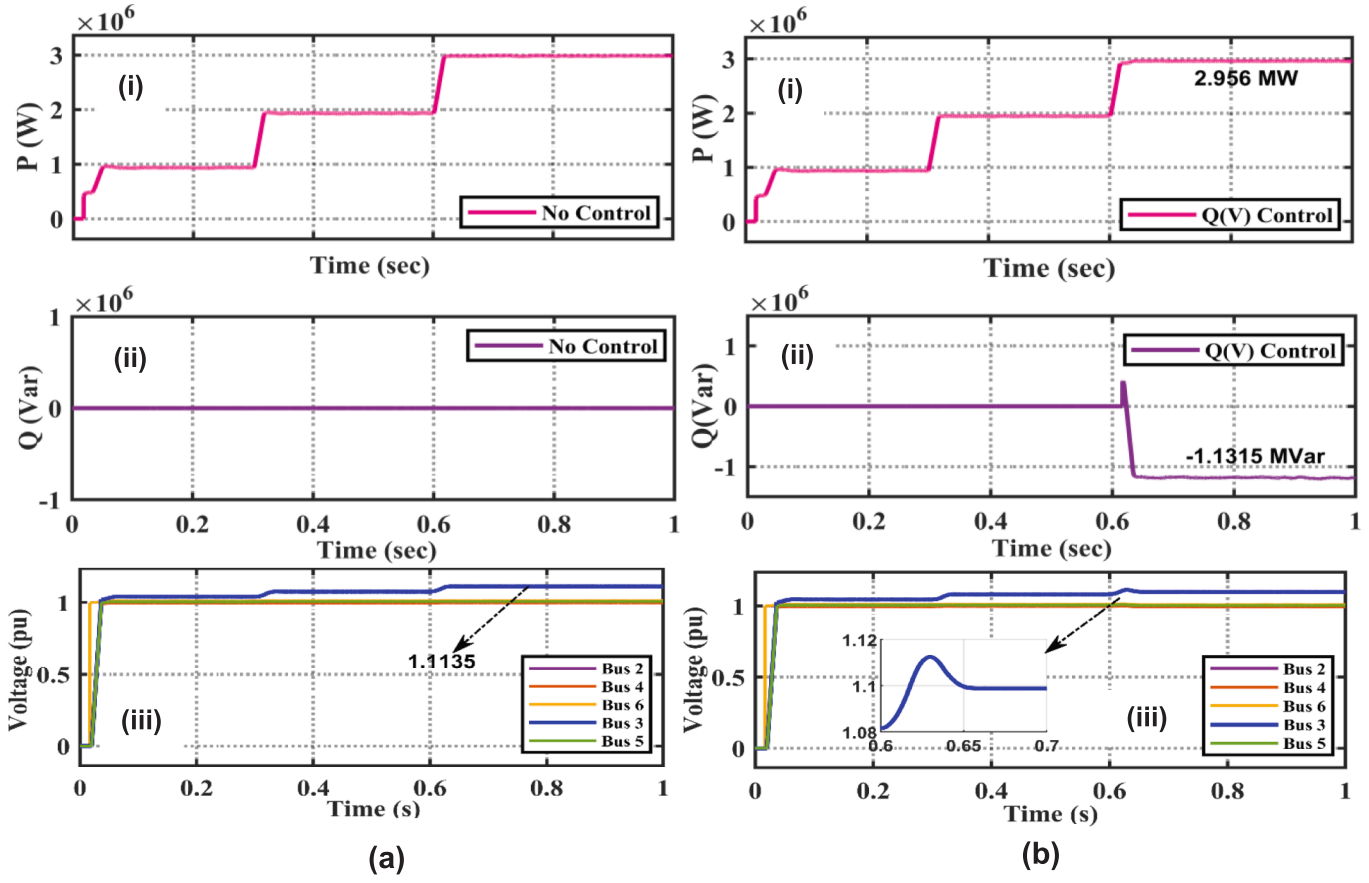

Fig. 17. Voltage and power response for Case 1 (a) No control (b)Data driven Volt-Var Control (Q(V)).

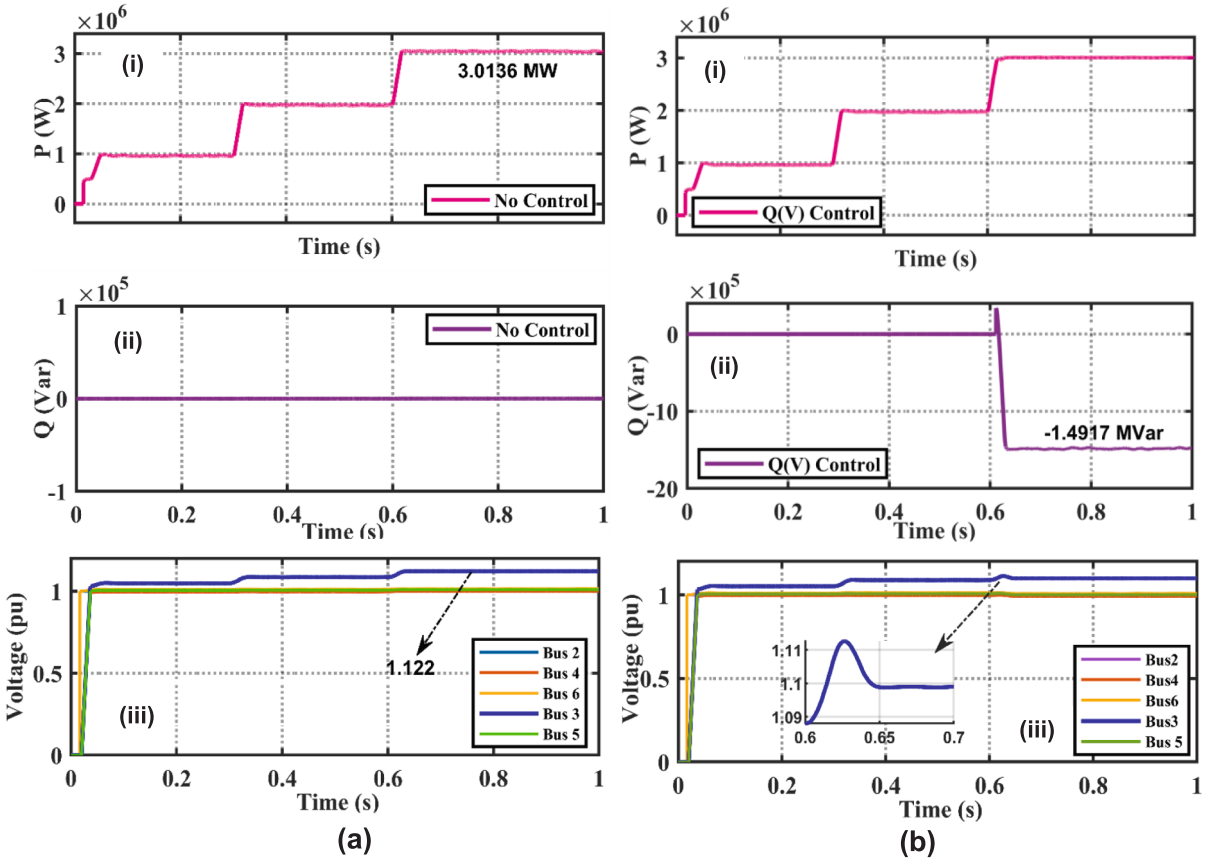

Fig. 18. Voltage and power response for Case 2 (a) No control (b) Data driven Volt-Var Control (Q(V)).

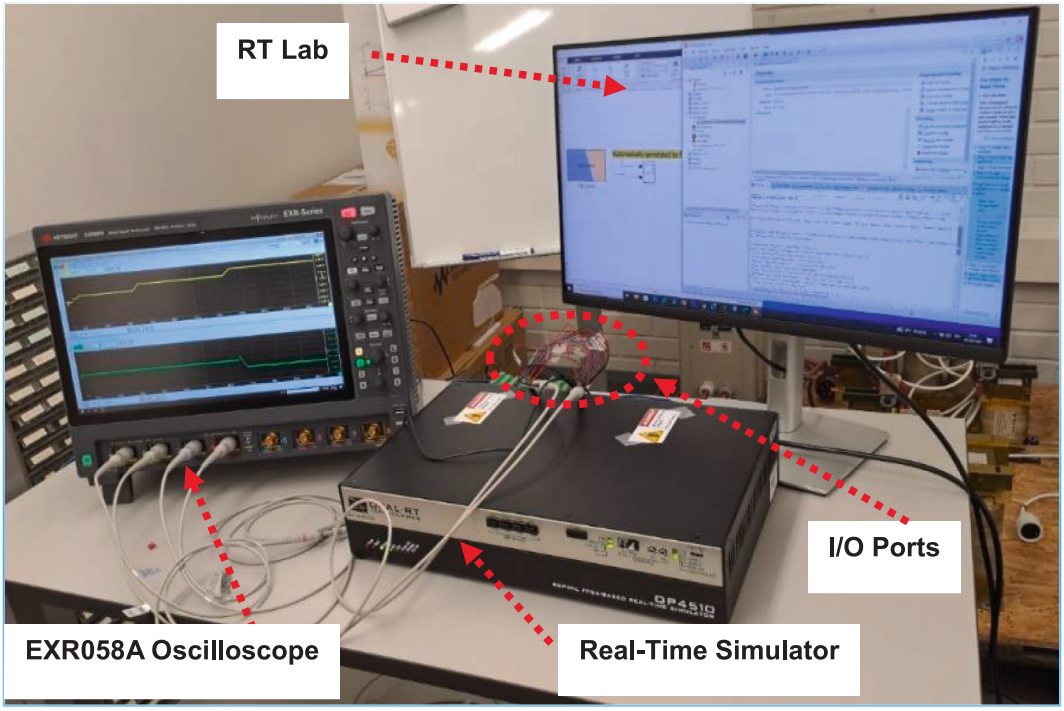

Fig. 19. Hardware setup for real-time simulations.

output ports of the OP4510.

The results obtained, as shown in Figs. 20 and 21, provide real-time validation of the simulated model, confirming its effectiveness under conditions closely resembling real-world operation. Specifically, for Volt–Var control of case 1 & 2 (Fig. 20(b) and Fig. 21(b)), the controller follows the active power reference points while absorbing

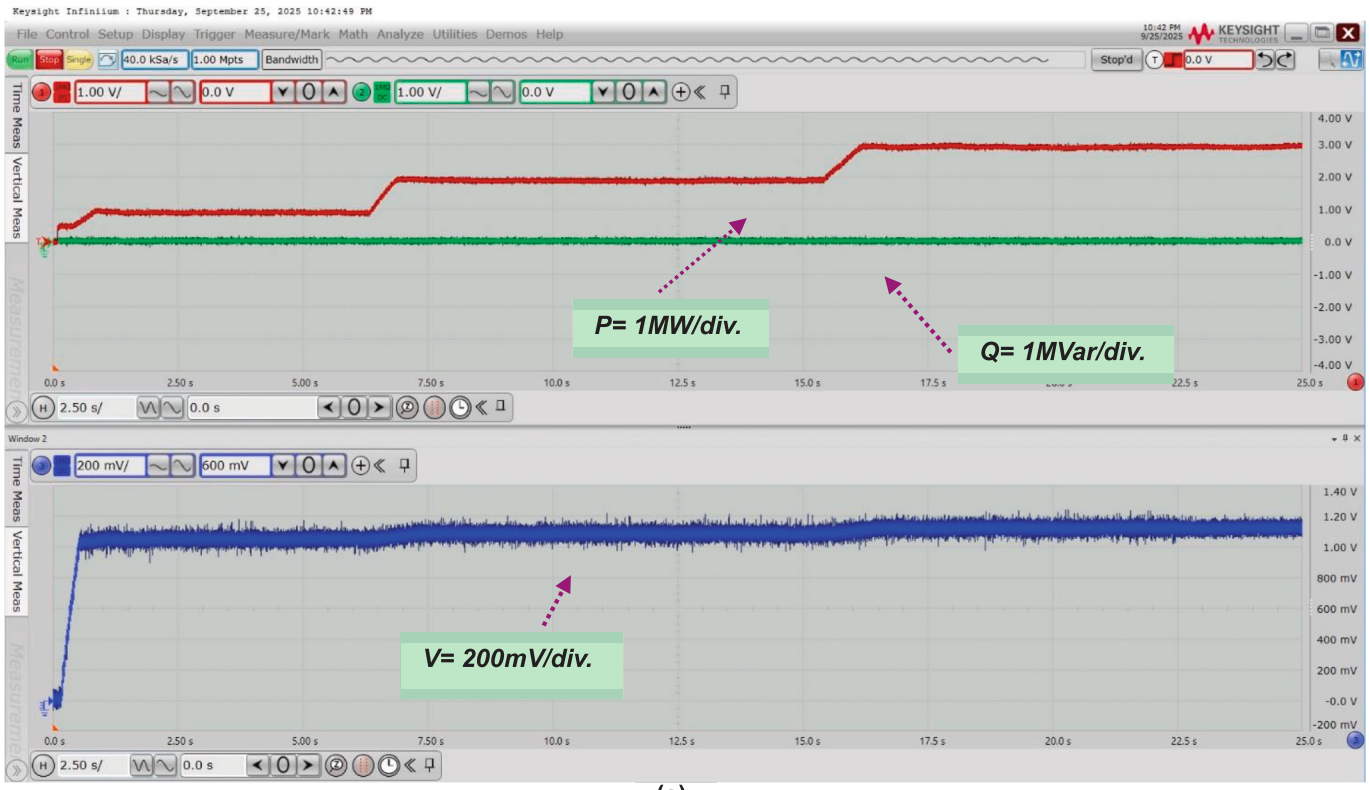

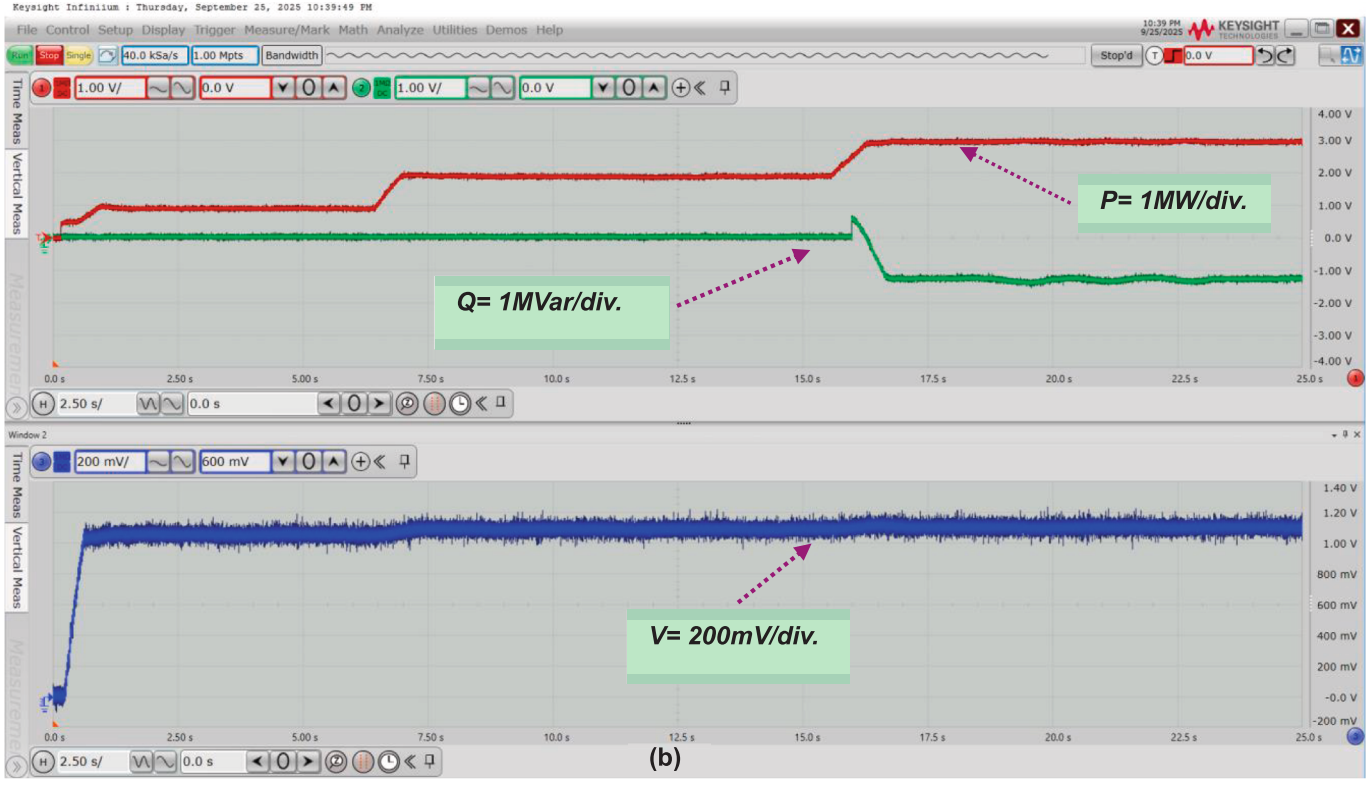

Fig. 20. Real time power response for case 1 (a) NC (b) Volt-Var control.

approximately 1.13 MVar and 1.49 Mvar of reactive power respectively to maintain the voltage within the permissible operating range. A clear consistency is evident between the MATLAB/Simulink simulations and the real-time results, demonstrating that under all DER penetration scenarios, the proposed MPC controller accurately tracks the active and reactive power setpoints, delivering a smooth and robust response. According to EN 50549, the maximum allowed tracking deviation is limited to 5 %. The presented results confirm that the proposed MPC controller meets these requirements, maintaining the reactive power response within the prescribed tolerance band with little to no

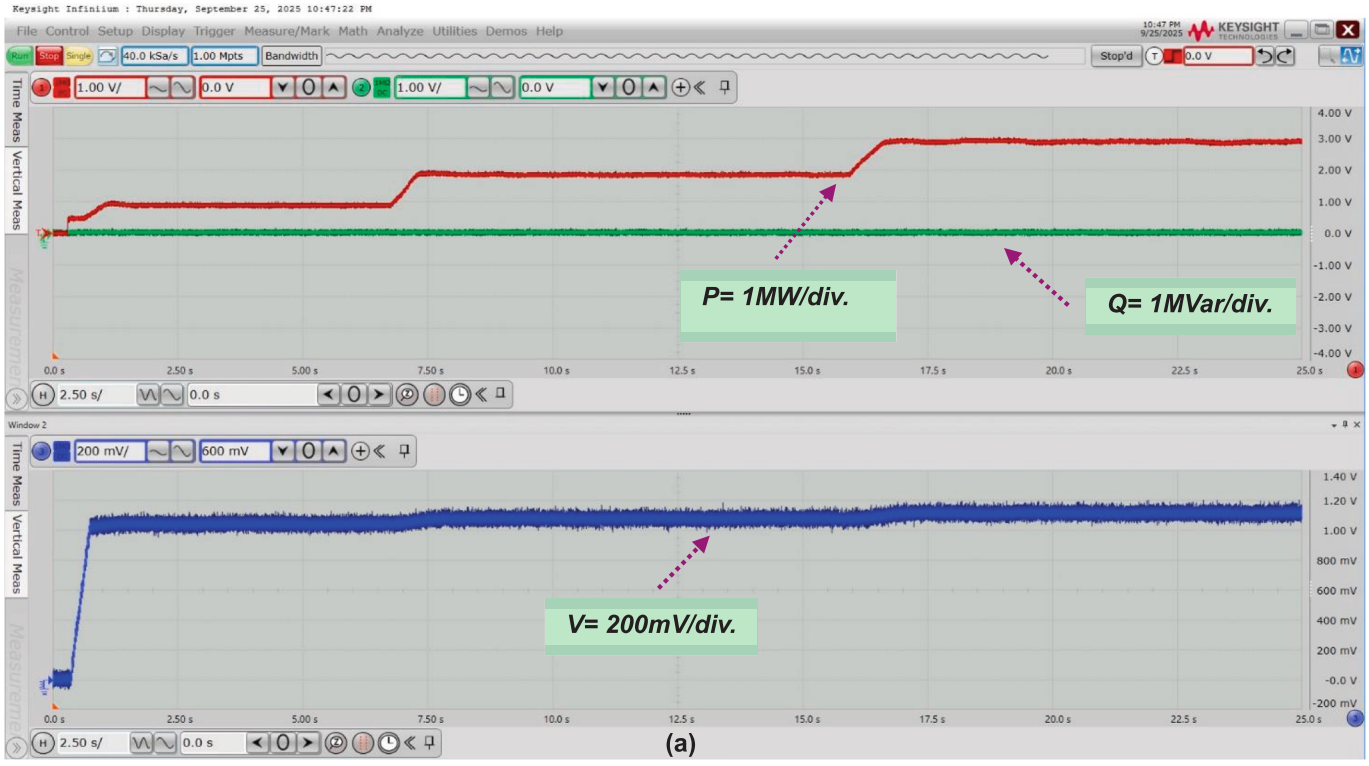

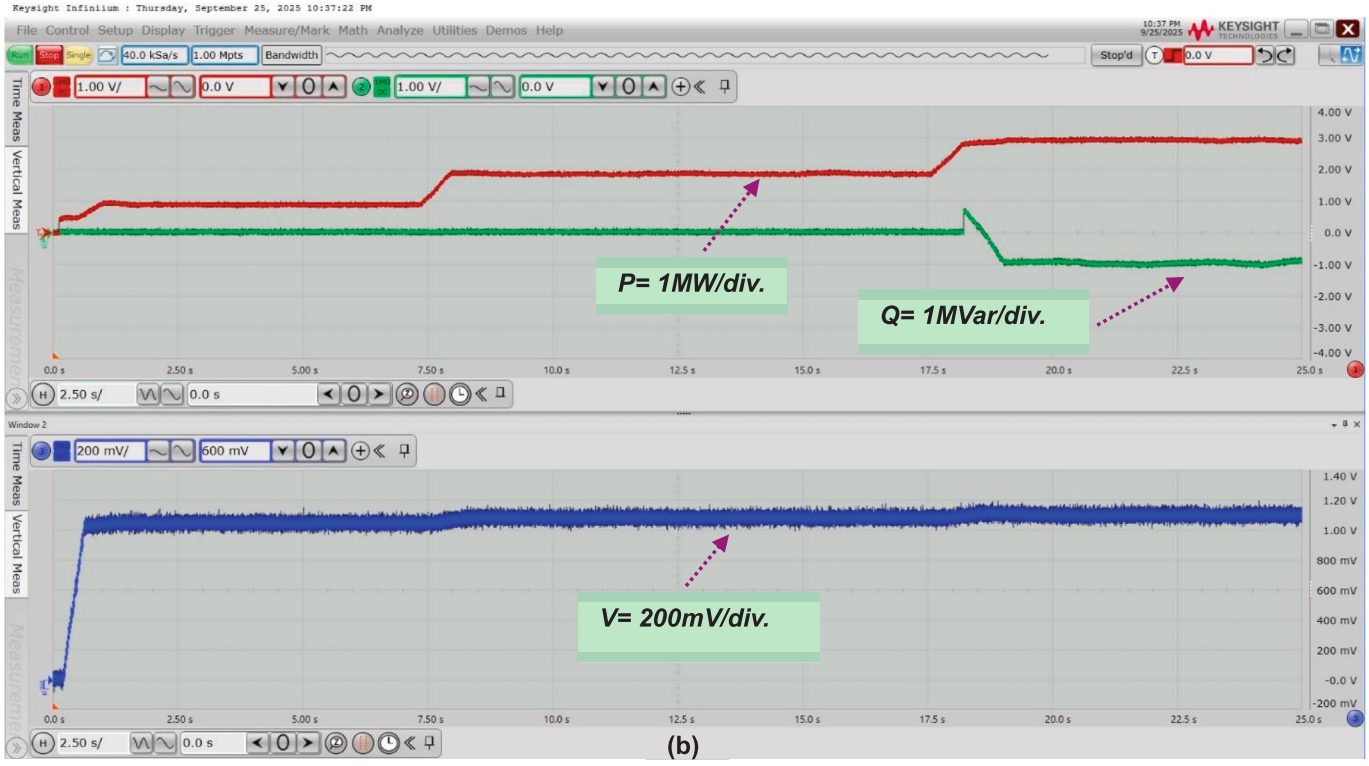

Fig. 21. Real time power response for case 2 (a) NC (b) Volt-Var control.

overshoot.

5. Discussions

In this study, a pre-trained deep learning model processes measurements from the test network to predict the optimal reactive power reference points. Since the deep learning model is trained offline, an important question arises regarding how often the model should be retrained in the context of rapidly evolving distribution systems. The frequency of data collection, device updates, and neural network retraining depends on factors such as grid dynamics, renewable energy penetration, and the ongoing evolution of distribution networks. As the penetration of renewable energy resources (RES) increases, grid dynamics can change significantly over short periods. The variable,

unpredictable, and intermittent nature of RES can impact the voltage profile and reactive power requirements. Therefore, in areas experiencing rapid renewable deployment, it is recommended to retrain the model on a quarterly or semi-annual basis.

Another key point of discussion is that this study presents a data-driven Volt–VAR control strategy designed in alignment with the requirements outlined in the EN 50549–2 standard. According to Article 4.7.2 of EN 50549–2, "*throughout the continuous (normal) operating frequency and voltage range, the generating plant shall be capable of delivering the requirements stipulated in* Fig. 2 (section 2.12)." Volt–VAR control is therefore intended to operate only within the continuous operating ranges. According to EN 50549, the continuous operating voltage range lies between 0.9p.u to 1.1p.u. Under abnormal or fault-level conditions, the Volt–VAR controller is not activated, and the generating unit follows the positive- and negative-sequence active/reactive power requirements defined in sections 4.7.4 and 4.9 of EN 50549–2.

Furthermore, in this study neural network predict active and reactive power reference points which are then supplied to the MPC controller. The MPC controller subsequently determines the optimal inverter switching states to directly regulate both active and reactive powers to meet the provided reference values. However, it is important to note that, as with all data-driven models, a certain level of prediction error is unavoidable in neural networks, especially when dealing with nonlinear systems. Therefore, even though controller performance remain stable and consistent, the accuracy of response is limited by the quality of prediction. The tracking error is due to the neural network limitations rather than deficiency in the controller itself. In future work, improvements in the data set, along with the integration of Physics-Informed Machine Learning models, could help mitigate prediction errors. By embedding physical laws, grid constraints, and Volt–VAR characteristics directly into the learning process, Physics-Informed Machine Learning approaches could lead to more accurate predictions and, ultimately, improved controller performance.

6. Conclusions

In this study, data-driven Volt-Var control is proposed for managing reactive power, with the goal of mitigating overvoltage issues and enhancing hosting capacity. A quantized deep learning model, trained offline using historical load and generation scenarios, processes real-time measurements from the test network to predict the optimal reactive power reference points which are supplied to D-FCS-MPC controller. The major conclusions are:

- Volt-Var curves generated using real-world load and generation scenarios exhibit nonlinear behavior.
- The QCNN model showcase efficient prediction performance under varying load and generation conditions achieving a Normalized Mean Squared Error (NMSE) of 0.0272, comparable to the 0.0271 NMSE of the standard 1D CNN model.
- Quantization results in a tenfold reduction in model size, making the QCNN model well-suited for deployment on resource-constrained edge devices.
- Under various DER penetration scenarios, the D-FCS-MPC controller gives a smooth and robust control response within the allowed tolerance levels mentioned in EN 50549–2 grid codes.

Furthermore, the research provides detailed HC analysis of the Sundom Grid (SSG), covering aspects from initial planning to the Volt-Var based control implementation. A Modified Reptile Search Algorithm (MRSA) is proposed to identify optimal size, location, dynamic deadband ranges, and slopes for maximizing hosting capacity. The major conclusions are:

- As the distance from the substation increases, the maximum HC value decreases.
- Higher HC values are attained by placing a single DER unit at a suitable location, instead of deploying multiple DER units along the feeder.
- When smart inverter (SI) Volt-Var control mode is activated, HC increases by 45.858 %.
- MRSA achieves an average improvement of 0.49 % in HC value compared to the PSO algorithm and demonstrates robust global optimization capabilities, surpassing other algorithms in terms of precision, reliability, and overall effectiveness.

CRediT authorship contribution statement

Muhammad Kamran Khan: Writing – original draft, Software, Methodology, Investigation, Conceptualization. **Kimmo Kauhaniemi:** Writing – review & editing, Validation, Supervision, Resources, Project administration, Funding acquisition, Formal analysis, Conceptualization. **Hannu Laaksonen:** Writing – review & editing, Validation, Resources, Formal analysis. **Muhammad Hamza Zafar:** Software, Formal analysis, Data curation.

Declaration of competing interest

The authors declare that they have no known competing financial interests or personal relationships that could have appeared to influence the work reported in this paper.

Acknowledgements

This work was carried out under projects titled Smart Grid 2.0 and Grid Code Certification by Simulation, with financial support provided by Business Finland under Grant #1386/31/2022 and Grant #2452/31/2024.

Data availability

Data will be made available on request.

References

[1] Mousa HHH, Mahmoud K, Lehtonen M. A comprehensive review on recent developments of hosting capacity estimation and optimization for active distribution networks. IEEE Access 2024:1.
[2] "The interconnection bottleneck." [Online]. Available: https://www.cleanegroup.org/wp-content/uploads/Interconnection-Bottleneck.pdf.
[3] Qamar N, Arshad A, Mahmoud K, Lehtonen M. Hosting capacity in distribution grids: a review of definitions, performance indices, determination methodologies, and enhancement techniques. Energy Sci Eng 2023;11(4):1536–59. https://doi.org/10.1002/ese3.1389.
[4] Ismael SM, Abdel Aleem SHE, Abdelaziz AY, Zobaa AF. State-of-the-art of hosting capacity in modern power systems with distributed generation. Renew Energy 2019;130:1002–20. https://doi.org/10.1016/j.renene.2018.07.008.
[5] Matevosyan J, et al. A future with inverter-based resources: finding strength from traditional weakness. IEEE Power Energ Mag 2021;19(6):18–28.
[6] Aboshady FM, Pisica I, Zobaa AF, Taylor GA, Ceylan O, Ozdemir A. Reactive power control of pv inverters in active distribution grids with high PV penetration. IEEE Access 2023;11:81477–96. https://doi.org/10.1109/ACCESS.2023.3299351.
[7] Dong C, et al. Renewable energy hosting capacity assessment in distribution networks based on multi-strategy improved whale optimization algorithm. IET Renew Power Gener 2024. https://doi.org/10.1049/rpg2.12994.
[8] Koirala A, Van Acker T, D'hulst R, Van Hertem D. Hosting capacity of photovoltaic systems in low voltage distribution systems: a benchmark of deterministic and stochastic approaches. Renew Sustain Energy Rev 2022;155:111899. https://doi.org/10.1016/j.rser.2021.111899.
[9] Golnazari R, Hasanzadeh S, Heydarian-Forushani E, Kamwa I. Coordinated active and reactive power management for enhancing PV hosting capacity in distribution networks. IET Renew. Power Gener. 2025;19(1):e12773. https://doi.org/10.1049/rpg2.12773.
[10] Huy PD, Ramachandaramurthy VK, Yong JY, Tan KM, Ekanayake JB. Optimal placement, sizing and power factor of distributed generation: a comprehensive study spanning from the planning stage to the operation stage. Energy 2020;195:117011. https://doi.org/10.1016/j.energy.2020.117011.
[11] Santos BLM, Barbosa D, Barros LS, Moreira FA. Photovoltaic hosting capacity maximization of low-voltage distribution systems based on search of optimal power factor for interface inverters through particle swarm optimization. J Control

Autom Electr Syst 2023;34(6):1260–71. https://doi.org/10.1007/s40313-023-01043-z.
[12] Jaramillo-Leon B, Zambrano-Asanza S, Franco JF, Leite JB. Simulation-based optimization framework to increase distribution system photovoltaic hosting capacity through optimal settings of smart inverter Volt-VAr control function. Electr Pow Syst Res 2023;215:108971. https://doi.org/10.1016/j.epsr.2022.108971.
[13] Babu KR, Khatod DK. Analytical voltage sensitivity-based distributed Volt/Var control for mitigating voltage-violations in low-voltage distribution networks. Electr Pow Syst Res 2024;228:110015. https://doi.org/10.1016/j.epsr.2023.110015.
[14] Khan MK, Kauhaniemi K, Khan HS. Optimizing smart inverter control for improved distribution network hosting capacity: a model predictive control approach. Int J Electr Power Energy Syst 2025;165:110472. https://doi.org/10.1016/j.ijepes.2025.110472.
[15] Jaramillo-Leon B, Zambrano-Asanza S, Franco JF, Soares J, Leite JB. Allocation and smart inverter setting of ground-mounted photovoltaic power plants for the maximization of hosting capacity in distribution networks. Renew Energy 2024;223:119968. https://doi.org/10.1016/j.renene.2024.119968.
[16] Gush T, Kim C-H, Admasie S, Kim J-S, Song J-S. Optimal smart inverter control for PV and BESS to improve PV hosting capacity of distribution networks using slime mould algorithm. IEEE Access 2021;9:52164–76. https://doi.org/10.1109/ACCESS.2021.3070155.
[17] Chang GW, Chinh NC, Sinatra C. Equilibrium optimizer-based approach of PV generation planning in a distribution system for maximizing hosting capacity. IEEE Access 2022;10:118108–22. https://doi.org/10.1109/ACCESS.2022.3220256.
[18] Rocabert J, Luna A, Blaabjerg F, Rodríguez P. Control of power converters in Ac microgrids. IEEE Trans Power Electron 2012;27(11):4734–49. https://doi.org/10.1109/TPEL.2012.2199334.
[19] Azab M. High performance decoupled active and reactive power control for three-phase grid-tied inverters using model predictive control. Prot Control Mod Power Syst 2021;6(1):25. https://doi.org/10.1186/s41601-021-00204-z.
[20] Maharjan S, Khambadkone AM, Peng J-C-H. Robust constrained model predictive voltage control in active distribution networks. IEEE Trans Sustain Energy 2021;12(1):400–11. https://doi.org/10.1109/TSTE.2020.3001115.
[21] Yang Y, Yeh H-G, Doan SH. Model predictive control via PV-based VAR scheme for power distribution systems with regular and unexpected abnormal loads. IEEE Syst J 2020;14(1):689–98. https://doi.org/10.1109/JSYST.2018.2880362.
[22] Singh S, Pamshetti VB, Singh SP. Time horizon-based model predictive Volt/VAR optimization for smart grid enabled CVR in the presence of electric vehicle charging loads. IEEE Trans Ind Appl 2019;55(6):5502–13. https://doi.org/10.1109/TIA.2019.2928490.
[23] Mabrook MM, Donkol AA, Mabrouk AM, Hussein AI, Barakat M. Enhanced the hosting capacity of a photovoltaic solar system through the utilization of a model predictive controller. IEEE Access 2024;12:62480–91. https://doi.org/10.1109/ACCESS.2024.3392645.
[24] Chathurangi D, Jayatunga U, Perera S, Agalgaonkar AP, Siyambalapitiya T. Comparative evaluation of solar PV hosting capacity enhancement using Volt-VAr and Volt-Watt control strategies. Renew Energy 2021;177:1063–75. https://doi.org/10.1016/j.renene.2021.06.037.
[25] Allahmoradi S, Afrasiabi S, Liang X, Zhao J, Shahidehpour M. Data-Driven Volt/VAR optimization for modern distribution networks: a review. IEEE Access 2024;12:71184–204. https://doi.org/10.1109/ACCESS.2024.3403035.
[26] Gupta S, Kekatos V, Chatzivasileiadis S. Optimal design of Volt/VAR control rules of inverters using deep learning. IEEE Trans Smart Grid 2024;15(5):4731–43. https://doi.org/10.1109/TSG.2024.3381984.
[27] Sun X, Qiu J, Tao Y, Zhao J. Data-driven combined central and distributed Volt/Var control in active distribution networks. IEEE Trans Smart Grid 2023;14(3):1855–67. https://doi.org/10.1109/TSG.2022.3213587.
[28] Singhal A, Ajjarapu V, Fuller J, Hansen J. Real-time local Volt/Var control under external disturbances with high PV penetration. IEEE Trans Smart Grid 2019;10(4):3849–59. https://doi.org/10.1109/TSG.2018.2840965.
[29] Yu N, et al. Data-driven control, optimization, and decision-making in active power distribution networks. Appl Energy 2025;397:126253. https://doi.org/10.1016/j.apenergy.2025.126253.
[30] Wang H, Yao Y, Zhao J, Ding F. Data-driven mean-corrected recursive estimation-based optimal DER dispatch for distribution system voltage control. IEEE Trans Sustain Energy 2025:1–12. https://doi.org/10.1109/TSTE.2025.3570218.
[31] Selim A, Ye Y, Zhao J, Yang B. Scalable Volt-VAR optimization using RLlib-IMPALA framework: a reinforcement learning approach for solar-powered grids. Sol Energy 2025;288:113255. https://doi.org/10.1016/j.solener.2025.113255.
[32] Sun X, Qiu J, Zhao J. Optimal local Volt/Var control for photovoltaic inverters in active distribution networks. IEEE Trans Power Syst 2021;36(6):5756–66. https://doi.org/10.1109/TPWRS.2021.3080039.
[33] Sandeep Ayyagari K, Gonzalez R, Jin Y, Alamaniotis M, Ahmed S, Gatsis N. Learning reactive power control polices in distribution networks using conditional value-at-risk and artificial neural networks. J Mod Power Syst Clean Energy 2023;11(1):201–11. https://doi.org/10.35833/MPCE.2022.000477.
[34] Miao L, Peng Y, Li Z, Xi W, Cai T. Data-driven Volt/Var control based on constrained temporal convolutional networks with a corrective mechanism. Electr Pow Syst Res 2023;224:109738. https://doi.org/10.1016/j.epsr.2023.109738.
[35] Zambri NA, Mohamed A, Wanik MZC. Performance comparison of neural networks for intelligent management of distributed generators in a distribution system. Int J Electr Power Energy Syst 2015;67:179–90. https://doi.org/10.1016/j.ijepes.2014.11.005.
[36] Sun X, Qiu J, Tao Y, Ma Y, Zhao J. A multi-mode data-driven volt/var control strategy with conservation voltage reduction in active distribution networks. IEEE Trans Sustain Energy 2022;13(2):1073–85. https://doi.org/10.1109/TSTE.2022.3149267.
[37] Shi N, Cheng R, Liu L, Wang Z, Zhang Q, Reno MJ. Data-Driven affinely adjustable robust Volt/VAr control. IEEE Trans Smart Grid 2024;15(1):247–59. https://doi.org/10.1109/TSG.2023.3270112.
[38] Takayama S, Ishigame A. Volt–Var curve determination method of smart inverters by multi-agent deep reinforcement learning. Int J Electr Power Energy Syst 2024;157:109888. https://doi.org/10.1016/j.ijepes.2024.109888.
[39] "FINGRID,16.11.2018, Grid Code Specifications for Power Generating Facilities, VJV2018." [Online]. Available: https://www.fingrid.fi/en/grid/grid-connection-agreement-phases/grid-code-specifications/grid-code-specifications-for-power-generating-facilities2/.
[40] "IEEE Standard for Interconnection and Interoperability of Distributed Energy Resources with Associated Electric Power Systems Interfaces.".
[41] "IEEE 2030. 5 common California IOU rule 21 implementation guide for smart inverters,Common Smart Inverter Profile Version 1.0, 2016." [Online]. Available: https://sunspec.org/wp-content/uploads/2017/02/CSIPImplementationGuide-v1-0.pdf.
[42] "Requirements for generating plants to be connected in parallel with distribution networks. Part 2: Connection to a MV distribution network. Generating plants up to and including Type B,SFS-EN 50549-2:2019.".
[43] Abualigah L, Elaziz MA, Sumari P, Geem ZW, Gandomi AH. Reptile Search Algorithm (RSA): a nature-inspired meta-heuristic optimizer. Expert Syst Appl 2022;191:116158. https://doi.org/10.1016/j.eswa.2021.116158.
[44] Harbola S, Coors V. One dimensional convolutional neural network architectures for wind prediction. Energy Convers Manag 2019;195:70–5. https://doi.org/10.1016/j.enconman.2019.05.007.
[45] Feng C, Wang Y, Chen Q, Ding Y, Strbac G, Kang C. Smart grid encounters edge computing: opportunities and applications. Adv Appl Energy 2021;1:100006. https://doi.org/10.1016/j.adapen.2020.100006.
[46] G. K. Thiruvathukal, Y.-H. Lu, J. Kim, Y. Chen, and B. Chen, *Low-Power Computer Vision: Improve the Efficiency of Artificial Intelligence*, 1st ed. Boca Raton: Chapman and Hall/CRC, 2022. https://doi.org/10.1201/9781003162810.
[47] Yan S, Yang Y, Hui SY, Blaabjerg F. A review on direct power control of pulsewidth modulation converters. IEEE Trans Power Electron 2021;36(10):11984–2007. https://doi.org/10.1109/TPEL.2021.3070548.
[48] Hu J, Zhu J, Dorrell DG. Model predictive control of grid-connected inverters for PV systems with flexible power regulation and switching frequency reduction. IEEE Trans Ind Appl 2015;51(1):587–94. https://doi.org/10.1109/TIA.2014.2328785.
[49] Saremi S, Mirjalili S, Lewis A. Grasshopper optimisation algorithm: theory and application. Adv Eng Softw 2017;105:30–47. https://doi.org/10.1016/j.advengsoft.2017.01.004.
[50] Kennedy J, Eberhart R. Particle swarm optimization. In: Proceedings of ICNN'95 - International Conference on Neural Networks. Perth, WA, Australia: IEEE; 1995. p. 1942–8. https://doi.org/10.1109/ICNN.1995.488968.
[51] Zhang J, Zhao J, Cheng G, Rouhani A, Chen X. Explainable multi-fidelity Bayesian neural network for distribution system state estimation. Appl Energy 2025;392:125972. https://doi.org/10.1016/j.apenergy.2025.125972.
[52] Zhang J, Zhao J, Yang J, Zhao J. Deep multi-fidelity bayesian data fusion for probabilistic distribution system voltage estimation with high penetration of PVs. IEEE Trans Power Syst 2024;39(2):3661–72. https://doi.org/10.1109/TPWRS.2023.3295795.
[53] Sayeh KF, Tamalouzt S, Ziane D, Benyahia N, Belaid SL. A novel fuzzy-logic-improved direct power control strategy for DFIG-based wind turbine through real-time OPAL-RT validation. Int J Electr Power Energy Syst 2025;172:111317. https://doi.org/10.1016/j.ijepes.2025.111317.
[54] Khan MK, Kauhaniemi K, Laaksonen H, Hassan MA. Review of recent developments in grid codes: focus on compliance testing and grid-forming inverter-based resources. Renew Sustain Energy Rev 2026;227:116509. https://doi.org/10.1016/j.rser.2025.116509.